Received: 15 December 2017 | Revised: 30 January 2018 | Accepted: 30 January 2018

DOI: 10.1002/cne.24406

RESEARCH ARTICLE

WILEY JCN RESEARCH IN SYSTEMS NEUROSCIENCE THE JOURNAL OF COMPARATIVE NEUROLOGY

Neuroanatomical details of the lateral neurons of *Drosophila melanogaster* support their functional role in the circadian system

Frank K. Schubert[1] | Nicolas Hagedorn[1] | Taishi Yoshii[2] | Charlotte Helfrich-Förster[1] | Dirk Rieger[1]

[1]Neurobiology and Genetics, Theodor-Boveri Institute, Biocenter, University of Würzburg, Würzburg 97074, Germany

[2]Graduate School of Natural Science and Technology, Okayama University, Okayama 700-8530, Japan

Correspondence
Dirk Rieger, Lehrstuhl für Neurobiologie und Genetik, Universität Würzburg, Biozentrum, Am Hubland, 97074 Würzburg, Germany.
Email: dirk.rieger@biozentrum.uni-wuerzburg.de

Funding information
Deutsche Forschungsgemeinschaft (DFG), Collaborative Research Center, Grant/Award Number: SFB 1047 "Insect timing", project A3

Abstract

Drosophila melanogaster is a long-standing model organism in the circadian clock research. A major advantage is the relative small number of about 150 neurons, which built the circadian clock in *Drosophila*. In our recent work, we focused on the neuroanatomical properties of the lateral neurons of the clock network. By applying the multicolor-labeling technique Flybow we were able to identify the anatomical similarity of the previously described E2 subunit of the evening oscillator of the clock, which is built by the 5th small ventrolateral neuron (5th s-LN_v) and one ITP positive dorsolateral neuron (LN_d). These two clock neurons share the same spatial and functional properties. We found both neurons innervating the same brain areas with similar pre- and postsynaptic sites in the brain. Here the anatomical findings support their shared function as a main evening oscillator in the clock network like also found in previous studies. A second quite surprising finding addresses the large lateral ventral PDF-neurons (l-LN_vs). We could show that the four hardly distinguishable l-LN_vs consist of two subgroups with different innervation patterns. While three of the neurons reflect the well-known branching pattern reproduced by PDF immunohistochemistry, one neuron per brain hemisphere has a distinguished innervation profile and is restricted only to the proximal part of the medulla-surface. We named this neuron "extra" l-LN_v (l-LN_vx). We suggest the anatomical findings reflect different functional properties of the two l-LN_v subgroups.

KEYWORDS

circadian clock neurons, *Drosophila melanogaster*, flybow, morphology, RRID: AB_760350, RRID: AB_2315460, RRID: AB_2314242, RRID: AB_2315311, RRID: AB_2314041, RRID: AB_300798,

Abbreviations: 5th s-LN_v, 5th small ventrolateral neuron; AME, accessory medulla; AME_{vel}, ventral elongation of the accessory medulla; AOT, anterior optic tract; AOTU, anterior optic tubercle; AVLP, anterior ventrolateral protocerebrum; AVP, anterior visual pathway; BU, bulb; Ca, mushroom body calyx; CRY, Cryptochrome; *cry-G80*, *cry-Gal80* (Repressor of Gal4); DenMark, dendritic marker; DN_{1a}, anterior dorsal neurons 1; DN_{1p}, posterior dorsal neurons 1; DN_2, dorsal neurons 2; DN_3, dorsal neurons 3; *DvPdf-G4*, *DvPdf-Gal4* driver (*Pdf*-promotor from *Drosophila virilis*); E-cells, evening cells; EGFP, enhanced green fluorescent protein; E-oscillator, evening oscillator; *Flybow*, refers to the Flybow system; *FB2.0B*, *UAS-Flybow2.0B*; GFP, green fluorescent protein; ICL, inferior clamp; ITP, ion transport peptide; LD, light-dark; LCBR, lateral cell body rind; LH, lateral horn; l-LN_v, large ventrolateral neurons; l-LN_{vx}, "extra" l-LN_v; LN_d, dorsolateral neurons; LO, lobula; LPN, lateral posterior neurons; M7, margin 7 of the medulla (serpentine layer); *Mai179-G4*, *Mai179-Gal4 driver*; MB, mushroom body; MDC, middle dorsal commissure; ME, medulla; mTq, monomeric turquoise fluorescent protein; NGS, normal goat serum; nSyb, neuronal Synaptobrevin; OL, optic lobe; PBS, phosphat buffered saline; PBT, phosphat buffered saline with Triton-X; ; PDF, Pigment dispersing factor; *Pdf-G4*, *Pdf-Gal4* driver; *Pdf-G80*, *Pdf-Gal80* (Repressor of Gal4); PED, mushroom body peduncle; PER, Period; PI, pars interecerebralis; PLP-LOF, fascicle connecting the posterior lateral protocerebrum with the dorsomedial lobula; POC, posterior optic commissure; PVLP, posterior ventral protocerebrum; PLP, posterior lateral protocerebrum; *R6-G4*, *R6-Gal4* driver; *R16C05-G4*, *R16C05-Gal4* driver; *R54D11-G4*, *R54D11-Gal4* driver; rAVLPl, cell body rind, lateral to the anterior ventrolateral protocerebrum; rLHla, cell body rind, lateroanterior to the lateral horn; SEZ, subesophageal zone; SCL, superior clamp; SIP, superior intermediate protocerebrum; s-LN_v, small ventrolateral neurons; SLP, superior lateral protocerebrum; SMP, superior medial protocerebrum; TIM, Timeless; TLN, Telencephalin; TTLF, transcriptional translational feedback loop; *UAS*, upstream activating sequence

RRID: AB_2536611, RRID: AB_2534096, RRID: AB_141780, RRID: AB_2534121, RRID: AB_2536186, RRID: AB_2535812, RRID: AB_2535804

1 | INTRODUCTION

Endogenous circadian clocks enable organisms to predict and adapt to environmental 24h rhythms that are caused by the earth's rotation around its own axis. The hence resulting circadian rhythms in physiology and behavior persist even in the absence of environmental Zeitgebers under constant conditions. Over the past years, the molecular mechanism driving circadian rhythmicity, several interlocked transcriptional and translational feedback loops could be described in large detail for the common model organisms, for example, *Synechococcus elongatus*, *Neurospora crassa*, *Arabidopsis thaliana*, *Drosophila melanogaster*, and *Mus musculus* (reviewed by Brown, Kowalska, & Dallmann, 2012). In *Drosophila melanogaster* ca. 150 clock neurons in the central nervous system, named after their size and location, show oscillations of core clock gene expression (e.g., *period*, *timeless* and *clock*). The neurons are further subdivided according to their neurochemical content and so far described function. Classically, they are divided into four lateral and three dorsal groups. Two of the lateral groups, the small and the large ventrolateral neurons (s-LN_vs and l-LNv_s, respectively; Figure 1) express the neuropeptide pigment dispersing factor (PDF), which has been shown to be an important signaling molecule of the circadian clock that modulates the other PDF-responsive cell groups of the circadian system by slowing down their Ca^{2+} oscillations (Liang, Holy, & Taghert, 2016, 2017). Further, it has been shown that the four PDF expressing s-LN_vs are important to sustain rhythmicity in constant darkness (Helfrich-Förster, 1998; Renn, Park, Rosbash, Hall, & Taghert, 1999). Since the s-LN_vs are also important for the generation and proper timing of the morning activity peak, which is part of the characteristic bimodal locomotor activity pattern of *Drosophila melanogaster*, the small PDF cells are often referred to as M-cells (Morning oscillators, Main-pacemakers; Grima, Chélot, Xia, & Rouyer, 2004; Stoleru, Peng, Agosto, & Rosbash, 2004; Rieger, Shafer, Tomioka, & Helfrich-Förster, 2006). In contrast, the evening activity peak is generated and controlled by the so-called E-cells, which comprise the 5th PDF lacking s-LN_v, three Cryptochrome (CRY) expressing dorsolateral Neurons (LN_ds), three CRY lacking LN_ds, and six to eight dorsal neurons (DN_1). The classification in M- and E-cells in respect to the traditional dual-oscillator model (Pittendrigh & Daan, 1976), as well as more recent working models (Yao & Shafer, 2014) attribute the lateral clock neurons (LN_s) an essential role for the generation of the bimodal locomotor activity rhythm. The latter study nicely showed the diverse responsiveness of the CRY expressing E-cells to secreted PDF, suggesting that the E-oscillator is composed of different functional subunits (E1-E3; Yao & Shafer, 2014) and that the circadian system is more likely a multi-oscillator system (Rieger et al., 2006; Shafer, Helfrich-Förster, Renn, & Taghert, 2006; Yao & Shafer, 2014). The E-cells cannot only be distinguished by their properties, but also by their neurochemistry. The E1-oscillator consists of two CRY expressing LN_ds which coexpress the short neuropeptide F (sNPF; Johard et al., 2009; Yao & Shafer, 2014), a peptide that has been shown to have an implication in promoting sleep by an inhibitory effect of the s-LN_vs (Shang et al., 2013). Further, the two E1-cells express the receptor for PDF (PDFR) and are strongly coupled to the s-LN_vs' output (Yao & Shafer, 2014). The E2-oscillator comprises one CRY expressing LN_d and the PDF lacking 5th s-LN_v (Yao & Shafer, 2014). The two neurons also express the PDFR, but additionally contain the ion transport peptide (ITP), which gets rhythmically released in the dorsal brain to enhance evening activity and inhibit nocturnal activity (Hermann-Luibl, Yoshii, Senthilan, Dircksen, & Helfrich-Förster, 2014). The molecular oscillations of the E2-cells are less strongly coupled to the M-cells' output compared to the E1-cells (Rieger et al., 2006; Yao & Shafer, 2014). The three remaining CRY negative LN_ds lack PDFR expression and form the E3-unit, which is not directly coupled to the M-cells' PDF-signaling (Yao & Shafer, 2014).

In the last decade, much effort was expended on unravelling the function of individual clock neurons and neuronal subgroups on the single cell level as well as on the network level, but we still lack detailed anatomical data on the projection patterns of individual clock neurons. This is mainly due to the limitations of *Gal4* drivers and the fact that antibodies tend to label a number of cells where it might be difficult to follow their projections if they are overlapping. *Gal4* drivers are primarily designed to exploit promotors of known genes and therefore are often addressing subsets or groups of neurons, which show expression of the consulted gene.

To nonetheless investigate the projections of the lateral clock neurons, two elaborated approaches were taken by the group of Helfrich-Förster. First, Helfrich-Förster et al. (2007) generated $disco^{01}$/wild-type gynandromorphs to elucidate the arborizations of the l-LN_vs in more detail. The mosaic mutant flies allowed the analysis of the arborizations stemming from the PDF cells that were only present in one brain hemisphere (Helfrich-Förster et al., 2007). In the same study, they described the *R6-G4* enhancer trap line, which drives expression in the central brain exclusively in the PDF expressing s-LN_vs (Helfrich-Förster et al., 2007).

One year later, Yoshii and colleagues used the *Mai179-G4* enhancer trap line (Siegmund & Korge, 2001) to rescue Period protein (PER) expression in a per^{null} mutant background, which led to an accumulation of Timeless protein (TIM) in the cytoplasm of *Mai179-G4* negative cells (which include the CRY^- LN_ds) after 5 days in constant darkness. They were able to describe the LN_ds' initial projections in the dorsolateral brain with antibody stainings of the cytoplasmically accumulated CRY in the CRY expressing cells and of the accumulated TIM in the CRY lacking LN_ds, showing that only the CRY containing neurons project ventrally toward the accessory medulla (AME; Yoshii, Todo, Wülbeck, Stanewsky, & Helfrich-Förster, 2008; complemented by Johard et al., 2009), a small neuropil adjacent to the frontomedial edge

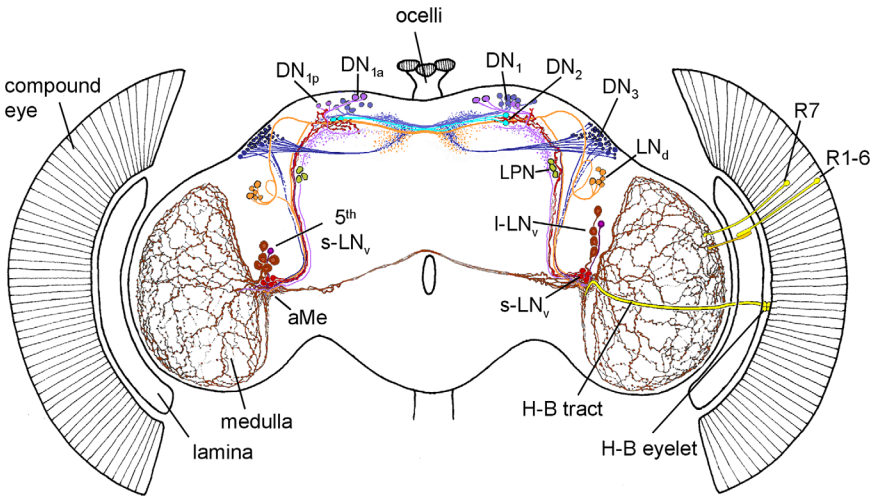

FIGURE 1 The known clock network of *Drosophila melanogaster*. Schematic overview shows the known arborizations of the clock neurons. The subgroups are named after their location in the brain; four small ventrolateral neurons (s-LN_vs, red), the 5th s-LN_v (dark violet), four large ventrolateral neurons (l-LN_vs, brown), six dorsolateral neurons (LN_ds, orange), three lateral posterior neurons (LPN, green), and ca. 60 neurons per hemisphere in three dorsal groups (DN_{1-3}, lilac, cyan, blue, respectively). The figure was taken from Helfrich-Förster et al. (2007) with permission

of the medulla, that is considered to be a major pacemaker and communication center of the clock neurons in various insects (Reischig & Stengl, 2003; Homberg, Reischig, & Stengl, 2003; Helfrich-Förster et al., 2007).

The mentioned publications outline the most detailed description of the LN_s' morphology to date (Figure 1), but we still cannot be sure whether anatomical differences are present within the mentioned neuronal subpopulations (s-LN_vs, l-LN_vs, CRY^+ LN_ds, and CRY^- LN_ds) and how far the projections of the LN_ds in the dorsal and ventral brain reach.

In our study, we used the revised multicolor reporter lines of the Flybow system to elude the previously mentioned limitations of *Gal4* lines and antibody stainings in regard to anatomical single cell studies (Hadjieconomou et al., 2011; Shimosako, Hadjieconomou, & Salecker, 2014). We increased the probability of single cell labeling by choosing the Flybow2.0B reporter construct, which carries a *FRT*-site flanked stop-codon upstream of the fluorescent protein sequences to restrict reporter expression. The stop-codon can be removed by Flp-recombination, induced by a heat shock-promotor controlled hs-Flp DNA-recombinase. During the heat-treatment of 37°C, we co-activate a modified Flp-recombinase that interacts with the fluorescence protein cassettes to alter the reporter expression. The combination of the Flybow technique with sufficiently specific Gal4 drivers for the LNs enabled us to answer three central questions that were bypassed by previous studies due to a lack of means: (a) are there any morphological differences within the subgroups of the lateral clock cells that can be used for further discrimination based on their anatomy? (b) which LN_ds are actually innervating the AME and how far-reaching are the projections in the dorsal brain? (c) can we identify unknown candidate regions for possible downstream contacts by analyzing the putative input and output sites of those neurons?

2 | MATERIAL AND METHODS

2.1 | Fly strains, genetic crosses and heat shock procedure

All fly strains used in this study were reared on standard cornmeal/agar medium with yeast at 25°C ± 0.2°C and 60% rH ± 5% rH in a LD cycle of 12:12 hr.

The experimental flies (Flybow-lines crossed to *Gal4*-drivers) were held on 18°C (18°C ± 0.2°C and 60% Rh ± 5% Rh in a LD cycle of 12:12) to prevent uncontrolled Flippase recombination events. From the used *Gal4* driver-lines *y w; Pdf-G4* (Renn et al., 1999), *w; DvPdf-G4* (Bahn, Lee, & Park, 2009), *w; +; R16C05-G4* and *w; +; R54D11-G4* (Pfeiffer et al., 2008), the latter three were crossed to a *10xUAS-myr::*

TABLE 1 Used Gal4-drivers and adressed clock neurons

	s-LN_vs	5th s-LN_v	l-LN_vs	LN_d CRY^+/ITP^+	LN_d CRY^+	LN_d CRY^-	$DN1_a$
Pdf-Gal4	+	−	+	−	−	−	−
DvPdf-Gal4	+	+	+	+	−	+	−
R16C05-Gal4	−	−	−	−	+	−	+
R54D11-Gal4	−	+	−	+	−	−	−

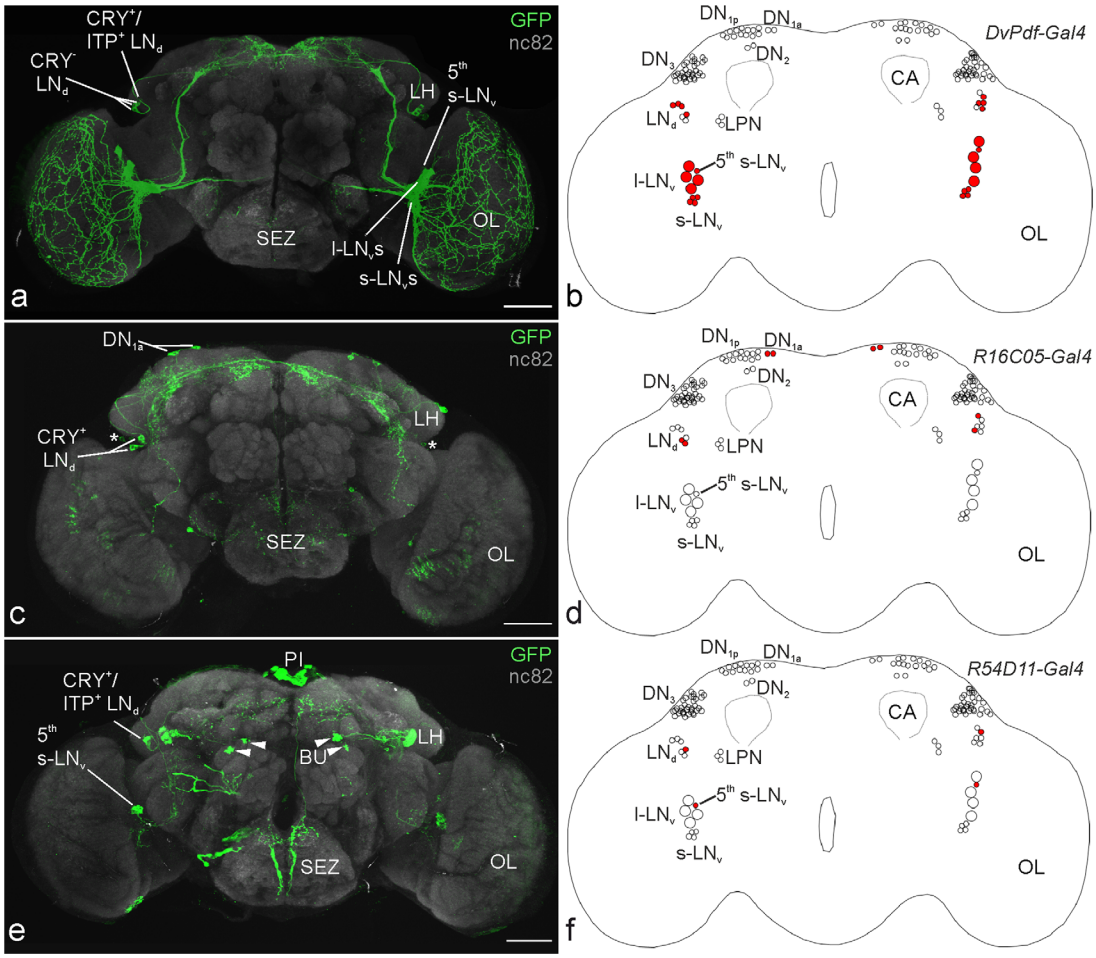

FIGURE 2 Characterization of the incompletely described *Gal4*-lines. *DvPdf-G4*: (a) GFP (green) and nc82 reference staining (gray) to show the overall expression pattern of the driver-line. (b) Overview of the clock neurons that are adressed by the *DvPdf-G4* driver (indicated in red). The line drives expression in all PDF$^+$ LN$_v$s, as well as in the 5th s-LN$_v$, three CRY$^-$ LN$_d$s, and the CRY/ITP-coexpressing LN$_d$. *R16C05-G4* driver line: (c) GFP (green) and nc82 neuropil staining (gray). (d) Overview of the clock neurons that are included in the *R16C05-G4* line (indicated in red). Alongside the two CRY$^+$/ITP$^-$ LN$_d$s, two anteriorly located dorsal neurons (DN$_{1a}$) are addressed per hemisphere. *R54D11-G4* driver: (e) GFP expression (green) with nc82 neuropil staining (gray). (f) The driver includes the two only two ITP expressing clock neurons, the 5th s-LN$_v$ and one LN$_d$ (indicated in red). BU, bulb; CA, calyx; LH, lateral horn; OL, optic lobe; PI, pars intercerebralis; SEZ, subesophageal zone. Scale bars = 50 μm

GFP reporter (Pfeiffer et al., 2010) and stained for the clock components TIM, PDF, ITP, and CRY to analyze their incompletely described expression patterns (Table 1, Figure 2, red cells). To build a driver stock for usage with the Flybow system, we balanced all above mentioned *Gal4* drivers and crossed them to *y w; hs-mFlp5^{MH12}/CyO; TM2/TM6B* (Shimosako et al., 2014) or to *y w; GlaBc/CyO; hs-mFlp5^{MH3}/TM6B* (Shimosako et al., 2014) depending on which chromosome the *Gal4* insertion was located. Experimental flies were obtained by crossing the balanced *Gal4*/hs-mFlp5 lines to either *hs-Flp^1; +; FB2.0B^{49b}* (Shimosako et al., 2014) or to *hs-Flp^1; FB2.0B^{260b}; +* (Shimosako et al., 2014) virgins.

The parental flies of the final crossing were transferred into new vials every 24 hr for seven consecutive days. Three heat shocks were applied for 45–60 min each at different developmental stages to each vial to induce Flp-recombinase activity. The adult flies were dissected and the brains got immunolabeled with anti-GFP, anti-mCherry, and anti-nc82 antibody-solution (Table 2).

To reveal the post- and presynaptic sites of the neurons of interest, we crossed the *Gal4*-drivers to *UAS*-DenMark::mCherry (Nicolaï et al., 2010) and *UAS*-nSyb::EGFP (Zhang, Rodesch, & Broadie, 2002), respectively. For analyzing the 5th s-LN$_v$ and the CRY$^+$/ITP$^+$ LN$_d$, we first crossed *pdf-G80* (Stoleru et al., 2004) into the *R54D11-G4* line, to restrict the reporter expression to the PDF-negative cells only. Furthermore, we were able to specifically look at the synaptic sites of the CRY$^-$ LN$_d$s by combining the *DvPdf-G4* driver with *cry-G80* (Stoleru et al., 2004) before crossing them to the reporter lines.

2.2 | Immunohistochemical staining

After eclosion, the experimental flies were entrained to a LD cycle of 12:12 for 4–5 days. Subsequently, the flies were collected at ZT 23 (1 hr before lights on) and the whole animals were fixed in 4% paraformaldehyde in phosphate buffered saline (PBS, pH 7.4) for 2.5 hr in darkness. After rinsing the flies with PBS (5 × 10 min), the brains were

TABLE 2 Used primary and secondary antibodies

Antibody	Source	Final concentration	Host species	Reference
anti-PDF-C7	DSHB	1:4.000	Mouse	Deposited by J. Blau 2005 RRID: AB_760350
anti-TIM	I. Edery	1:2.000	Rat	Sidote, Majercak, Parikh, and Edery, (1998) RRID: AB_2315460
anti-CRY	T. Todo	1:1.000	Rabbit	Yoshii et al. (2008) RRID: AB_2314242
anti-ITP	H. Dircksen	1:10.000	Rabbit	Dircksen, Tesfai, Albus, and Nässel, (2008) RRID: AB_2315311
nc82 (anti-Brp)	MAB Hofbauerlibrary	1:100	Mouse	Hofbauer (1991) RRID: AB_2314041
anti-GFP	Abcam	1:2.000	Chicken	RRID: AB_300798
anti-mCherry	ThermoScientific	1:2.000	Rat	RRID: AB_2536611
AlexaFluor488 (anti-chicken)	ThermoScientific	1:200	Goat	RRID: AB_2534096
AlexaFluor555 (anti-mouse)	ThermoScientific	1:200	Goat	RRID: AB_141780
AlexaFluor568 (anti-rat)	ThermoScientific	1:200	Goat	RRID: AB_2534121
AlexaFluor635 (anti-rabbit)	ThermoScientific	1:200	Goat	RRID: AB_2536186
AlexaFluor647 (anti-rabbit)	ThermoScientific	1:200	Goat	RRID: AB_2535812
AlexaFluor647 (anti-mouse)	ThermoScientific	1:200	Goat	RRID: AB_2535804

dissected in PBS containing 0.1% Triton-X100 (PBT 0.1%, pH 7.4) before they were incubated in the blocking solution (5% normal goat serum, NGS, in PBT 0.5%) at 4°C overnight. At noon of the following day we transferred the brains into the primary antibody solution containing 5% NGS and 0.02% NaN_3 in 0.5% PBT (for further information on which antibodies were used see Table 2) and incubated for two nights at 4°C. After washing in PBT 0.1% (5 × 10 min), they were incubated in the secondary antibody solution (see Table 2 for used antibodies) for 3 hr at room temperature. After incubation, the brains were washed in PBT 0.1% (3 × 10 min) and rinsed two more times for 10 min in PBS. Subsequently, all brains were aligned on a specimen slide and embedded in Vectashield 1000 mounting medium (Vector Laboratories, Burlingame, CA). The samples were stored at 4°C in darkness until scanning.

2.3 | Confocal microscopy and image processing

Fluorescence protein expression and antibody staining was visualized with a Leica TCS SP8 confocal microscope (Leica Microsystems, Wetzlar, Germany) equipped with hybrid detectors, photon multiplier tube, and a white light laser for excitation, using the laser and detector settings as described in Shimosako et al. (2014). We used a 20-fold glycerol immersion objective (HC PL APO, Leica Microsystems, Wetzlar Germany) for whole mount scans and obtained confocal stacks with 2 μm z-step size and 1024 × 512 pixels. For magnifications, we used a 63-fold glycerol objective (HC PL APO, Leica Microsystems, Wetzlar Germany) and scanned the brains with a resolution of 2048 × 2048 pixels and a slice-thickness of 1 μm. For the PMT all focal planes were scanned four times and the frames were averaged to reduce background noise. The HyD were used with photon counting mode and each focal plane was scanned and accumulated four times. The obtained confocal stacks were maximum projected and analyzed with Fiji ImageJ (Schindelin et al., 2012). Besides contrast, brightness and color scheme adjustments, no further manipulations were done to the confocal images, if not stated otherwise.

We used the Neuron2-APP2 implementation from the vaa3D software package for the 3D reconstructions of single cells (Peng, Ruan, Long, Simpson, & Myers, 2010; Peng, Bria, A., Zhou, Z., Iannello, G., & Long, 2014a; Peng et al., 2014b; Xiao & Peng, 2013). The tracing files were imported and adjusted in Fiji and visualized via the 3D viewer plug-In (Schmid, Schindelin, Cardona, Longair, & Heisenberg, 2010). Sample alignment to the Janelia Farm Research Campus standard brain (JFRC2) was carried out in Fiji with the computational morphometry tool kit graphical user interface plug-In (CMTK GUI, Rohlfing & Maurer, 2003; Jefferis et al., 2007).

2.4 | Cell-size estimation, statistical analysis and graphical editing

For the comparison of cell sizes among the different clock neurons, we measured the maximum diameter of identified cells in Fiji using the standard measurement tools. We exclusively measured cells that were labeled with cytosolic or membrane-bound markers and where we could clearly identify the orientation and therefore the maximum diameter. Using a one-way ANOVA under Bonferroni post-hoc correction (α=0.05), cell size diameters were tested for significant differences. Statistical analysis was performed using the SPSS 23 (IBM, Chicago, IL) software after testing datasets for normal distribution (Shapiro-Wilkinson test). Schematic overviews, graphs and figures were edited and arranged using CorelDRAW Graphics Suite X8 (Corel Corporation Ltd., Ottawa, Canada).

3 | RESULTS

3.1 | Characterization of the Gal4-lines

In order to analyze the morphology of the lateral clock neurons, we used suitable *Gal4*-Lines and identified the included cells by their neurochemistry. From this screen, we selected four driver lines that cover all lateral clock neurons of *Drosophila melanogaster* (Table 1).

The *Pdf-G4* line is already well-established and drives expression in the PDF expressing s-LN_vs and l-LN_vs (Renn et al., 1999). The expression pattern of the *DvPdf-G4* driver includes the PDF-cells, the PDF-negative 5th s-LN_v, and four LN_ds per hemisphere (Bahn et al., 2009; Guo, Cerullo, Chen, & Rosbash, 2014), of which three lack CRY expression, whereas the fourth coexpresses CRY and ITP (Table 1, Figure 2a,b).

The *R16C05-G4* line drives expression in two dorsal neurons and in two, rarely in three, dorsolateral neurons (Figure 2c). Four clock neurons per brain hemisphere could be identified by TIM immunoreactivity (Figure 2d). The dorsal neurons, which expressed GFP, CRY, and TIM, were located in the anterior part of the brain, hence they were identified as $DN1_a$ (Figure 2c). Two TIM immunoreactive neurons were situated ventrally to the lateral horn in the dorsolateral brain. These neurons belong to the LN_d cell cluster and express CRY but not ITP. A third dorsolateral non-clock neuron appears to be weakly GFP positive in some brains (asterisk in Figure 2c), however, the soma of this neuron is smaller and therefore distinguishable from the dorsolateral clock cells and the projections are almost not visible due to the weak GFP expression. Additionally, there are two non-clock cells innervating the subesophageal zone (SEZ) in the ventral brain, and sparse GFP signal in the optic lobes (OL; Figure 2c).

Reporter expression with the *R54D11-G4* line (Figure 2e,f) was observed in the pars intercerebralis (PI), the SEZ, and in some small cells that were located anteriorly in the brain and innervate the bulb (BU; Figure 2e). In addition, two neurons per brain hemisphere were also expressing GFP and could be identified as clock neurons by consistent labeling with TIM immunostaining. The two lateral clock neurons both express the circadian photoreceptor CRY and co-labeling with PDF and TIM anti-sera revealed that the ventrally located neuron is the PDF lacking 5th s-LN_v. To confirm this result and to further characterize the included CRY expressing LN_d, we also co-stained for the circadian clock component ITP, which is reported to be expressed by one LN_d and the 5th s-LN_v exclusively among the clock cells (Johard et al., 2009). Actually both cells of interest were immunoreactive to ITP anti-sera, showing that the *R54D11-G4* line includes the 5th s-LN_v and the ITP/CRY coexpresssing LN_d.

3.2 | Single cell morphology of the lateral clock neurons

3.2.1 | Differences within the l-LN_v cluster

The morphology of the PDF expressing lateral clock neurons has already been described in detail (Helfrich-Förster & Homberg, 1993; Helfrich-Förster, 1995; Helfrich-Förster et al., 2007). The M-cells (PDF expressing LN_vs) are a heterogeneous group of four small (s-LN_vs) and four large (l-LN_vs) ventrolateral neurons per brain hemisphere. The two subgroups show different projection patterns, but are considered to be indistinguishable within the sub clusters of s-LN_vs and l-LN_vs.

We used the *Pdf-G4* driver line to address only the PDF expressing s- and l-LN_vs for analysis with the Flybow reporter system. Since the projection pattern of PDF-cells is well known in respect to their location in the brain, we employed a commonly utilized PDF antibody for our counterstaining instead of a neuropil labeling compound, in order to examine whether the overall network looks regular.

Out of 275 brains with fluorescent protein expression in the s-LN_vs, only 14 brains showed individually labeled cells. Here we could not find any systematic morphological differences among them compared to the already known s-LN_v projection pattern (described in detail by Helfrich-Förster et al., 2007). In contrast the analysis of 166 single labeled l-LN_vs revealed a yet completely unknown morphological subclass of large ventrolateral clock neurons. One third of the analyzed l-LN_vs showed a restricted projection pattern on the surface of the ipsi- and contralateral ME compared to the so far described morphology (Figure 3c).

Due to the lack of further distinctive features we called the l-LN_v with its newly found characteristics "extra" l-LN_v (l-LN_vx) for the ease of discrimination. We think that there is only one l-LN_vx present in each hemisphere (10 single labeled l-LN_vx out of 166 analyzed l-LN_vs).

The majority of l-LN_vs (three out of four per hemisphere) show between four to five main projections on the surface of the ipsilateral ME. These projections originate from a side-branch (yellow 3 in Figure 3k) of the fiber that runs through the POC. In the contralateral hemisphere, between two and four main projections run onto the surface of the ME, which are further subdividing toward the distal part of the ME (Figure 3a,b). Both hemispheres are connected via a single projection of each l-LN_v that runs through the POC without additional branching in the central brain (Figure 3k).

The l-LN_vx shows the same initial branching pattern (shown in Figure 3k) as the other l-LN_vs, but innervates only the proximal area of the ME surfaces (Figure 3c,e). The two ME branches (blue 2 and yellow 3 in Figure 4k) bifurcate at the anteromedial edge of the ME, one branch runs ventrally whereas the other projects dorsally along the medial ME surface (Figure 3c).

Both l-LN_v types possess several fine fibers, originating from the first branching point, which invade the ipsilateral AME and proceed into the ME serpentine layer (Figure 3j). Furthermore, both l-LN_v subclasses contribute to the ventral elongation of the ipsilateral AME (AME_{vel}, Figure 3a, c). Notably, the projection in the AME_{vel} of the l-LN_vx is not as far-reaching as the one of the remaining l-LN_vs (Figure 3a, c). Therefore, the AME_{vel} of the l-LN_vx turns to the posterior part of the ME to a smaller extent compared to the residual l-LN_vs.

We can exclude the possibility that the morphology of the newly described l-LN_vx is due to optic lobe injury or impaired pathfinding, since we also obtained brains in which one l-LN_vx was individually labeled among few of the other l-LN_vs (Figure 3e–h). In these brains, the remaining l-LN_vs show their characteristic projection pattern without any abnormalities of the network on the surface of the ME

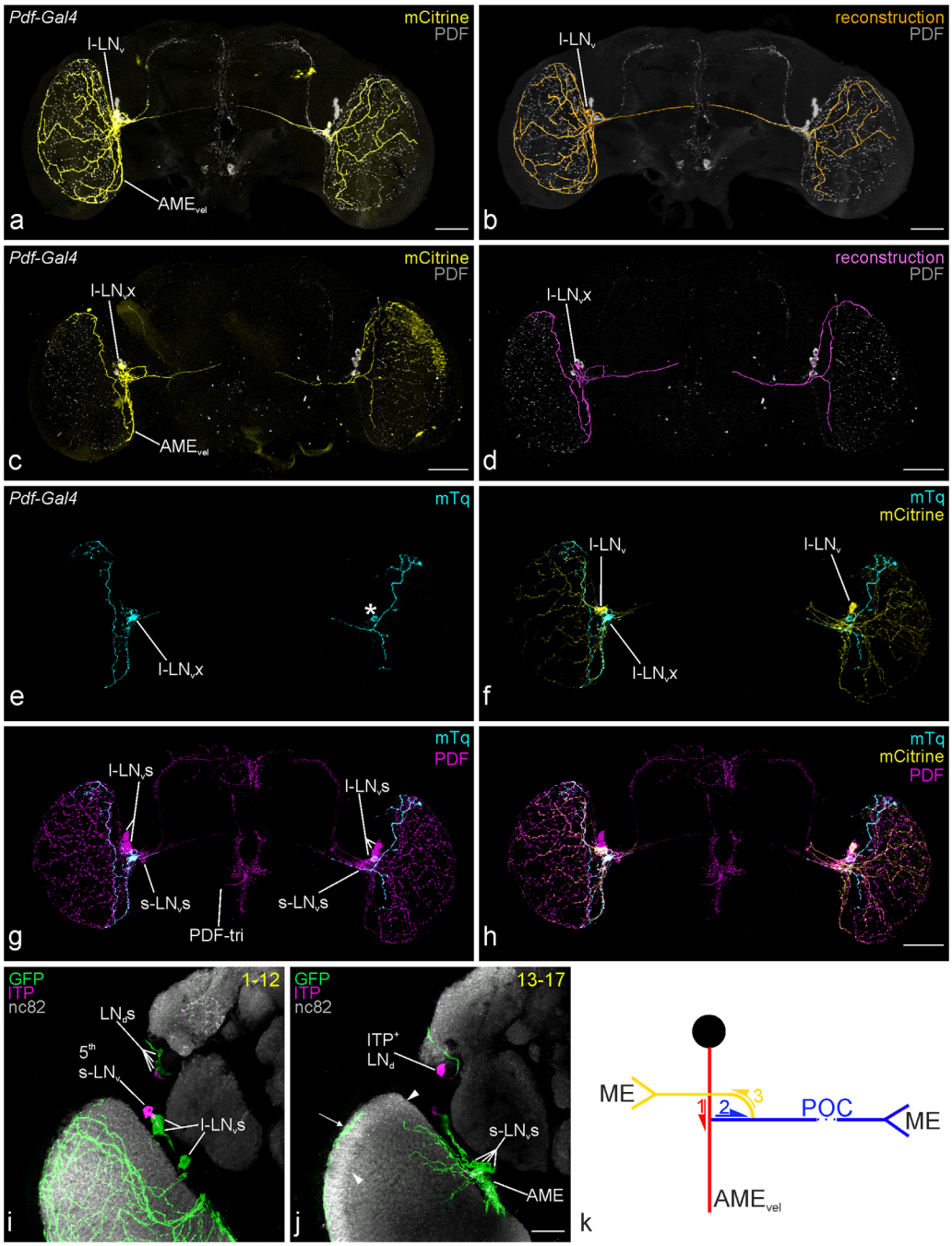

FIGURE 3 Heterogenic morphology of the large ventrolateral neurons. (a, b) Expression of mCitrine (yellow) in a single l-LN$_v$ and its reconstruction (orange) showing the already described morphology. (c, d) mCitrine expression (yellow) and reconstruction (magenta) of a single l-LNv showing the so far undescribed anatomy of a subtype of l-LNvs ("extra" l-LN$_v$, l-LN$_v$x) and the morphological heterogeneity within this neuronal group. (e–h) Control staining for l-LNv heterogeneity. Flybow reporter expression driven by *Pdf-G4*: (e) Single l-LNv expressing mTorquoise in the left brain hemisphere showing the newly found morphology. The cell in the right hemisphere (asterisk) is bleeding through from another channel, but all visible projections are stemming from the l-LN$_v$x. (f) Two l-LN$_v$s in the same brain expressed mCitrine (yellow), one cell in each hemisphere, showing the already described projection pattern. (g) Anti-PDF staining showing the well-characterized projection pattern of the PDF$^+$ LN$_v$s, confirming the structural integrity of the network. (h) Merge of the previous channels. (i, j) Projections of the l-LN$_v$s are extensively invading the serpentine layer of the medulla. The majority of l-LN$_v$ neurites run on the surface of the medulla (i; arrow in j), but a remarkable proportion is invading the serpentine layer (j). The boundary between the inner and outer layers can be seen in the dorsal and distal area of the medulla (indicated with arrowheads in j). (k) Schematic representation of the initial branching pattern of l-LN$_v$s. The primary projection (red) runs ventrally from the soma (black sphere) along the medial edge of the ipsilateral medulla and forms the ventral elongation of the accessory medulla (AME$_{vel}$). A secondary fiber (blue) branches off from the initial projection, runs through the posterior optic commissure (POC) and is thereby connecting both hemispheres, to eventually arborize onto the surface of the contralateral ME. The fiber network on the ipsilateral ME is built by the branches of a third side-projection (orange) which separates from the fiber that runs through the POC. Scale bars = 50 μm

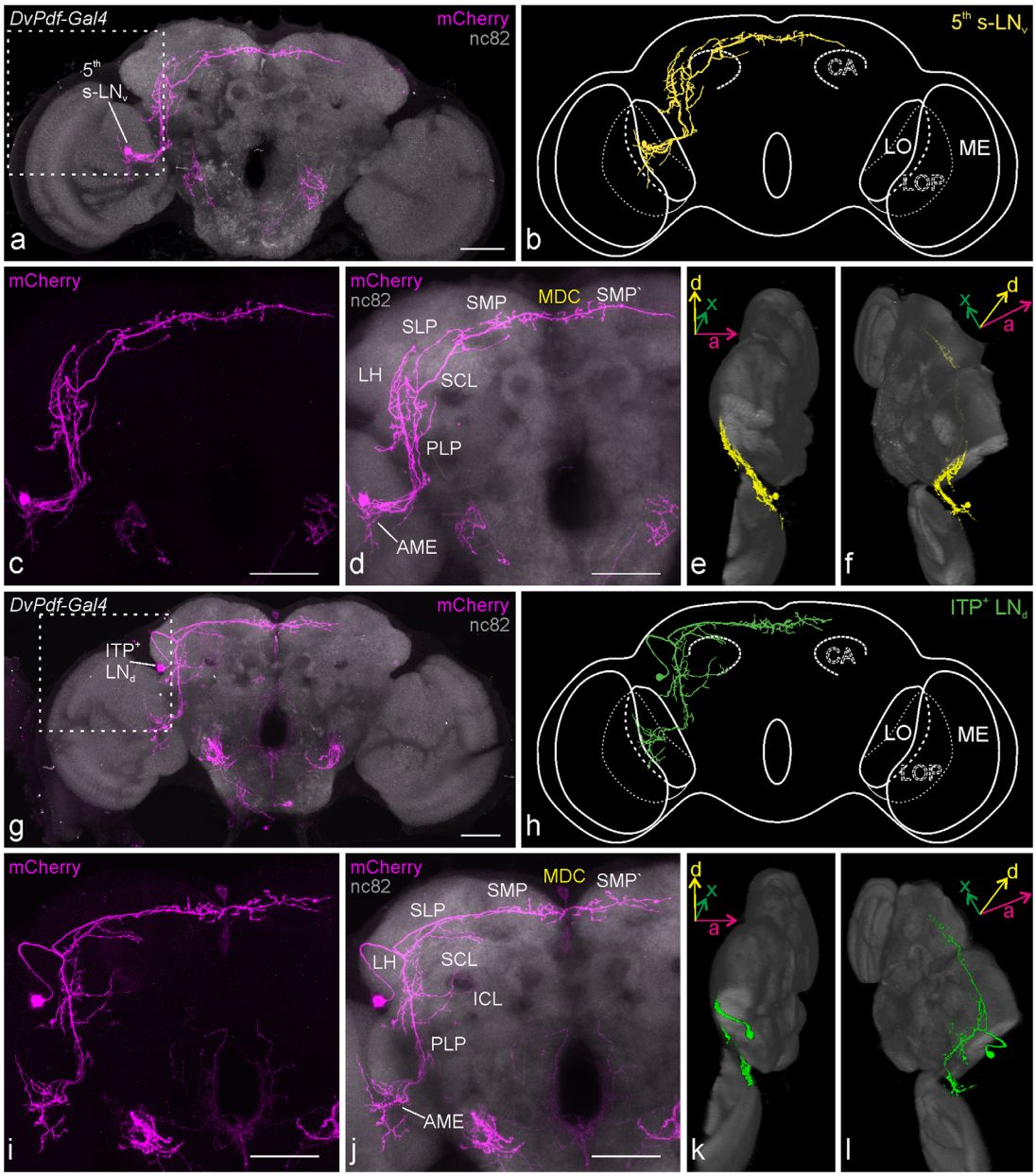

FIGURE 4 Projection pattern of the 5th s-LNv and the ITP expressing LNd. (a) Overview of the 5th s-LN_v expressing mCherry (magenta) and nc82 neuropil staining (gray). The part that was cut out for the 3D view (e, f) is shown by the dashed square. (b) Scheme of the 5th s-LN_v. (c-d) Magnification. (e, f) Anterior-lateral (e) and posterior-lateral (f) view of the 5th s-LN_v. The optic lobe of the left hemisphere was partly cut out (as indicated in a) for a better view on the soma and the initial branching. (g–l) Morphology of the CRY^+/ITP^+ LN_d. (g) Amplified mCherry expression (magenta) with nc82 neuropil staining (gray). The dashed square indicates the section that was cut out for the 3D view in (k) and (l). (h) Schematic overview of the same neuron. (i, j) Magnification. (k, l) Anterior-lateral (k) and posterior-lateral (l) view of the neuron and its location in the brain. The dorsal part of the left optic lobe was cut out (indicated in g) for improved visibility of the projections running toward the optic neuropils. Orientation of the brain (e, f and k, l) is declared by the coordinate system. a, anterior; d, dorsal; x, lateral axis. ME, medulla; LO, lobula; LOP, lobula plate; CA, calyx; AME, accessory medulla; PLP, posterior lateral protocerebrum; LH, lateral horn; SCL, superior clamp; ICL, inferior clamp; SLP, superior lateral protocerebrum; SMP, superior medial protocerebrum; MDC, middle dorsal commissure; SMP, superior medial protocerebrum of the contralateral hemisphere. Scale bars = 50 μm

(Figure 3f). Furthermore, the overall staining pattern against the PDF peptide was unaffected in flies where we found individually labeled l-LN_vx, showing that the overall network is intact and was not damaged during dissection of the brains (Figure 3g).

3.2.2 | Morphology of the 5th s-LN_v

The *DvPdf-G4* and the *R54D11-G4* driver lines were used to unravel the projection pattern of the so far poorly described 5th s-LN_v. By using the Flybow2.0B construct we received eight individually labeled

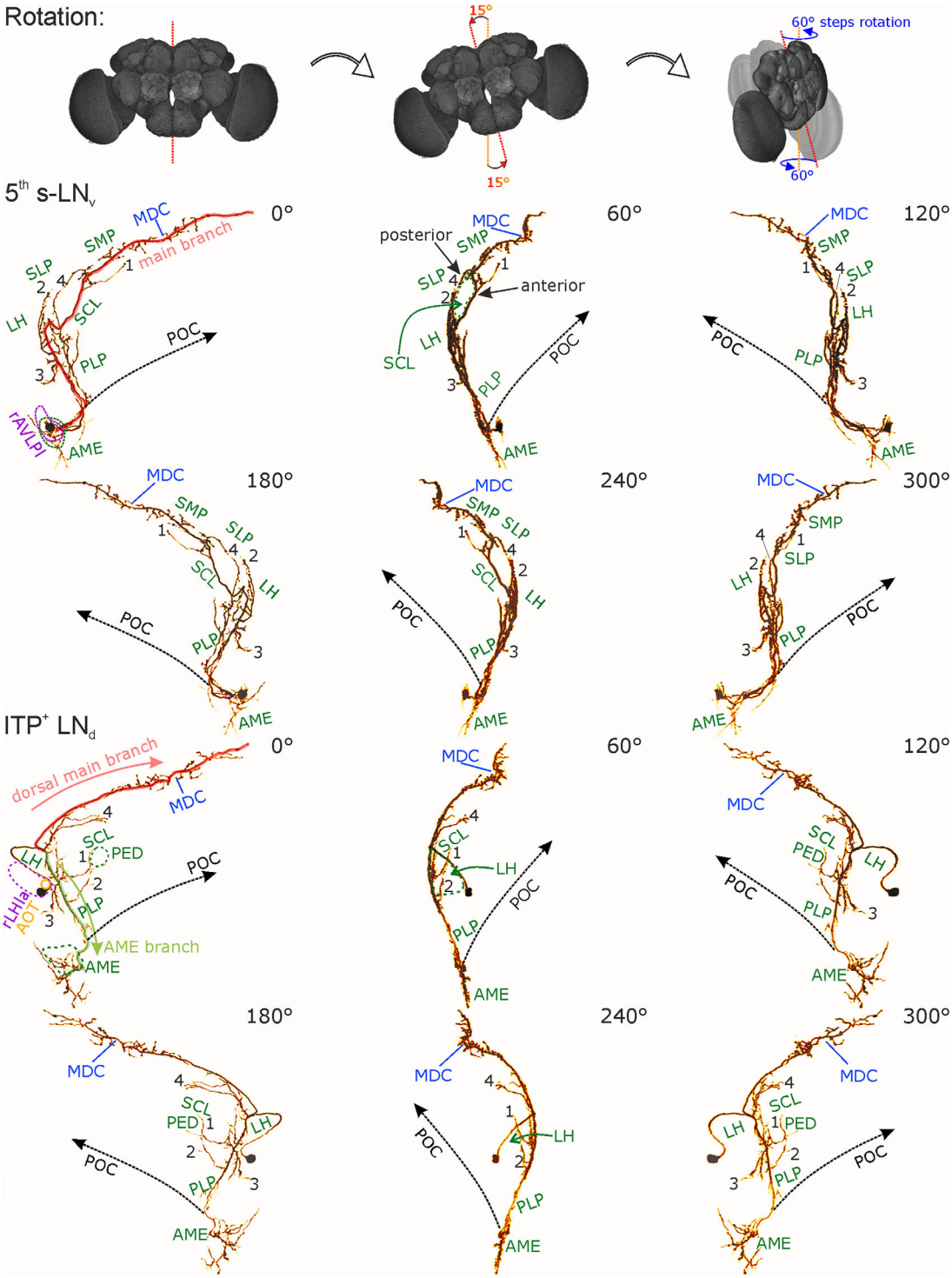

FIGURE 5 Characteristic anatomical features of the ITP expressing lateral clock cells. 5th s-LN_v single cell projection pattern rotated and viewed from different angles in 60° steps (upper two panels). In the plane view (0°) the main branch was labeled (red) and characteristic branches were numbered for further description (see maintext). For easier orientation, the dorsoventral midline is indicated (dashed blue line) and landmark fiber bundles are implied (POC, posterior optic commissure). Included neuropil structures are shown in dark green. The location of the cell body is highlighted in purple (rAVLPl). In the dorsal brain, the main projection reaches into the contralateral hemisphere via the middle dorsal commissure (MDC). Rotated ITP^+ LNd single cell projection pattern (lower panels). The dorsal and ventral main projections were labeled (red and light green, respectively) and characteristic branches were numbered for detailed description (see maintext). The dorsoventral midline (dashed blue line) and landmark fiber bundles are indicated (AOT, POC). Like the 5th s-LNv, the LN_ds' dorsal main projection is crossing the dorsoventral midline via the MDC (blue). AME, accessory medulla; AOT, anterior optic tract; rAVLPl; cell body rind lateral to the anterior ventrolateral protocerebrum; SCL, superior clamp; PED, mushroom body peduncle; rLHla, cell body rind lateroanterior to the lateral horn

5th s-LN$_v$s. Despite most analyzed samples showed only sparse labeling, the majority of specimen had more than one cell expressing the same fluorescence protein. Nonetheless, tracing the entire projections of a neuron was still feasible in brains where only one additional cell was labeled by the same reporter. Hereby it was possible to analyze the morphology of in total 19 5th s-LN$_v$s.

The soma of the neuron is situated in the LCBR medially to the anterior part of the ME and lateral to the AVLP (rAVLPl, Figure 4a; Figure 5, upper panel). Only few fibers run onto the surface of the ME after invading the AME. Most projections run along the medial edge of the ME at the level of the serpentine layer, which gets invaded by several fine fibers. The projections exit the AME along the initial part of the POC and run to the posterior side of the brain around the PVLP Figure 4d; Figure 5, upper panel). In the posterior brain, the main bundle leaves the POC and proceed dorsally into the PLP where the fibers start to branch. The neurites leave the POC either as a fascicle or as separate fibers, but there is always one main branch, that is slightly thicker than the others (Figure 5, upper panel). This main projection runs in parallel to the remaining fibers until it reaches the ventromedial LH (Figure 4d). There it turns and proceeds more anteriorly through the SCL into the SLP and SMP. In the SMP the neurite turns even more anterior, runs through the MDC into the contralateral SMP and then turns back to the posterior part of the brain. From here, the main branch projects to the center of the contralateral SLP. The majority of varicose endings that branch off the dorsal main projection can be observed in the SMP of both hemispheres.

A fine neurite (1, Figure 5, upper panel) separates from the main branch in the SCL and runs ventrally to the SIP into the ventrolateral SMP, where it usually reconnects with the main branch. A secondary neurite (2, Figure 5, upper panel), which originates from the main projection in the lateral PLP, runs into the ventral LH and furcates into small fibers that are terminating in the LH. Another secondary fiber (3, Figure 5, upper panel) branches off from the main projection in the dorsolateral PLP, proceeding lateral via the PLP-LOF to the LO.

The remaining neurites, which run through the PLP project to the dorsal brain in parallel to the main branch (4, Figure 5, upper panel). In the ventromedial LH, where the main branch turns to the anterior side, the other fibers proceed dorsal and run through the dorsolateral SCL into the SLP, where they are ending in close vicinity to the dorsal main branch.

3.2.3 | Morphology of the ITP and CRY coexpresssing LN$_d$

We employed two different *Gal4* lines to look at the arborization pattern of the only cell among the six LN$_d$s that is expressing ITP. The *DvPdf-G4* with a broad expression in the clock network and the *R54D11-G4* with a more narrow expression in only two clock neurons, the 5th s-LN$_v$ and the LN$_d$ of interest (Figure 2). Previously, it was shown that this cell has two main branches, one invading the superior neuropils of the brain and one running ventrally toward the AME (Helfrich-Förster et al., 2007; Johard et al., 2009). However, it was not described whether it actually innervates the AME, nor if it is projecting into the contralateral hemisphere in the dorsal brain.

We obtained 12 single labeled ITP expressing LN$_d$s of individual brains and, taken together with sparsely labeled brains, could analyze the morphology of 31 cells in detail.

The cell body of the neuron is situated at the posterior dorsolateral edge of the AVLP, close to the boundary between the anterior and posterior ventrolateral protocerebrum and in the LCBR, lateroanterior to the lateral horn (rLHla, Figure 4j; Figure 5, lower panel). Dorsally to the soma runs the AOT and the LH starts to expand on the posterior side (Figure 4j). Initially, the neuron projects medially around the AOT and is then proceeding dorsally on the anterior surface of the LH. The fiber runs around the LH to the posterior surface of the neuropil and branches there for the first time.

One main branch (AME branch, see Figure 5, lower panel) descends toward the AME and passes through the PLP, where it vastly branches. Three smaller neurites separate from the ventral main branch in the dorsal PLP. Two projections run medially, from which one encompasses the PED of the ipsilateral MB. The dorsal projection (1, Figure 5, lower panel) innervates the SCL, whereas the ventral one (2, Figure 5, lower panel) runs into the ICL. Another neurite proceeds more laterally (3, Figure 5, lower panel) and reaches from the PLP into the dorsomedial part of the LO via the PLP-LOF. The AME branch leaves the PLP along the POC and projects to the anterior part of the brain, running along the posterior surface of the PVLP. In the anterior brain, at the level of the boundary between the PVLP and the AVLP, the ventral main projection branches into the AME and from here into the serpentine layer and onto the surface of the ME.

The second main projection (dorsal main branch, Figure 5, lower panel) originates from the initial branching in the LH and innervates the superior neuropils. The neurite runs in the posterior part of the brain and therefore only innervates the SLP and the SMP, but not the SIP. The fiber crosses the dorsoventral midline and reaches into the contralateral hemisphere via the MDC. In the contralateral brain hemisphere, the neurite innervates the SMP and terminates a few microns after entering into the SLP. The dorsal main branch shows varicose endings in the SMP of both brain hemispheres, most of them are in close vicinity to the dorsoventral midline near the PI.

A second dorsal projection (Figure 5, lower panel), which also originates from the initial branching point in the posterior LH, runs in parallel to the dorsal main branch, but slightly more ventral. The neurite branches into two fibers that leave the medial center of the LH. The fiber that runs more dorsal compared to the other, projects between the dorsal boundary of the SCL and the ventral boundary of the SLP, and terminates in the ventral part of the SLP. The ventral fiber runs in parallel but slightly more anterior in the brain. It also projects between the ventral SLP and the dorsal SCL, but it ends in the dorsomedial SCL, close to the posterior edge of the SIP.

3.2.4 | Morphology of the two sNPF and CRY coexpressing LN$_d$s

The *R16C05-G4* driver line was used to disentangle the projections of the sNPF and CRY containing LN$_d$s from the remaining dorsolateral and dorsal clock neurons. In this driver line, only the two sNPF and CRY expressing LN$_d$s and the DN$_{1a}$s were addressed and there was

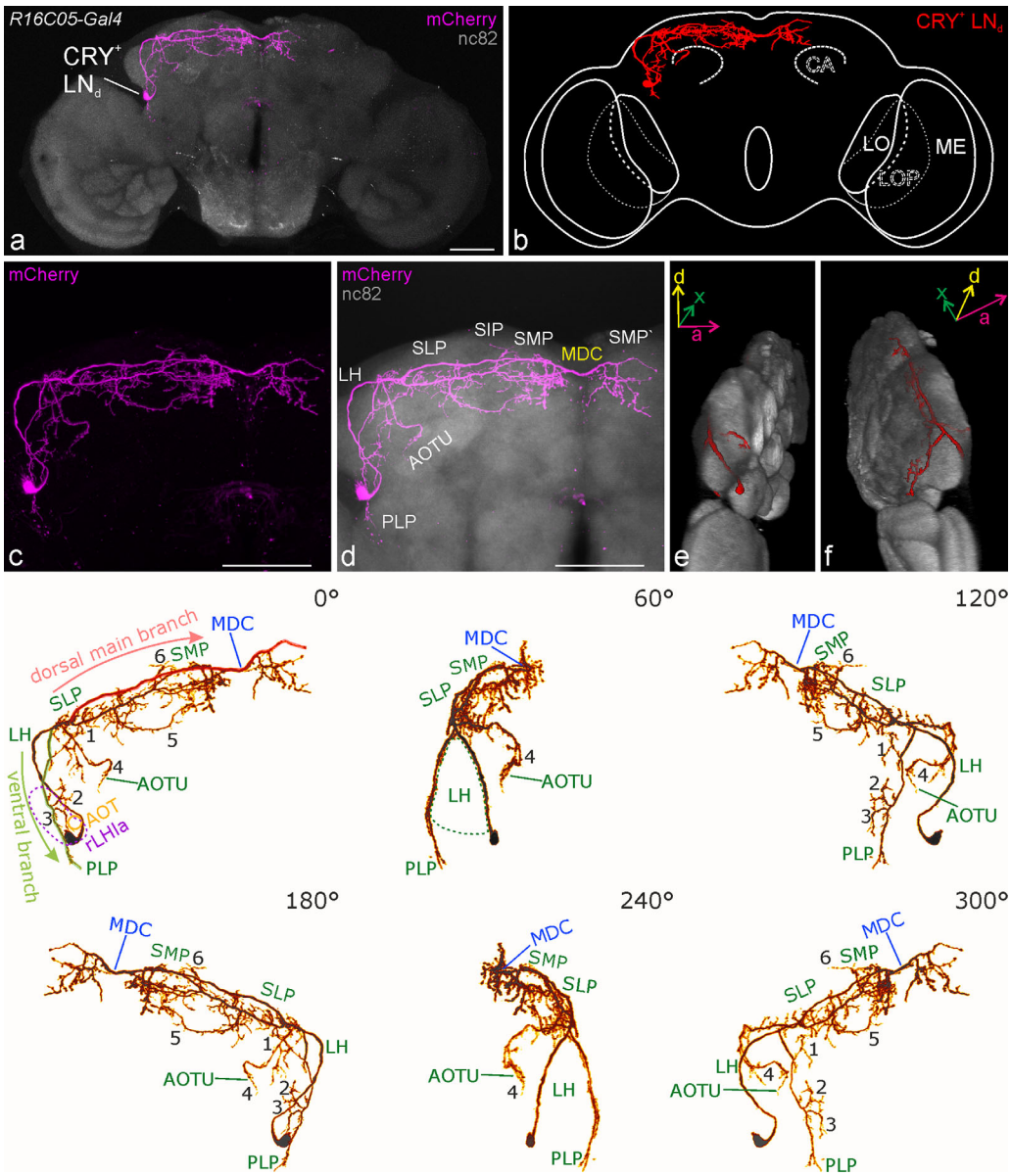

FIGURE 6 Morphology of the two sNPF$^+$/CRY$^+$ LN$_d$s. (a) Depiction of one of the two CRY$^+$ but ITP$^-$ LN$_d$s labeled with mCherry antibody (magenta) shown together with a nc82 neuropil staining (gray). (b) Schematic overview. (c, d) Magnification. (e, f) Anterior-lateral (e) and posterior lateral (f) view on the 3D brain. The orientation is indicated by the coordinate system. Rotated sNPF$^+$/CRY$^+$ LN$_d$ (lower panel). The dorsal and ventral main branches are labeled (red and light green, respectively) and characteristic branches were numbered for further description in the maintext. The dorsoventral midline is indicated (dashed blue line), and landmark fiber bundles are implied (AOT) for easier orientation. Additional information on neuropil structures are shown in dark green, whereas the location of the cell body is highlighted in purple (rLHla). The dorsal main projection contibutes to the MDC (blue) and passes into the contralateral hemisphere. a, anterior; d, dorsal; x, lateral axis. AOTU, anterior optic tubercle; AOT; anterior optic tract; ME, medulla; LO, lobula; LOP, lobula plate; CA, calyx; PLP, posterior lateral protocerebrum; LH, lateral horn; SLP, superior lateral protocerebrum; SIP, superior intermediate protocerebrum; SMP, superior medial protocerebrum; MDC, middle dorsal commissure; SMP, superior medial protocerebrum of the contralateral hemisphere; rLHla, cell body rind lateroanterior to the lateral horn. Scale bars = 50 μm

almost no further *Gal4* expression in the adult central brain (see Figure 2c). In total 101 sNPF/CRY coexpressing LN$_d$s were analyzed, from which 17 were individually labeled.

The two cell bodies of the CRY expressing LN$_d$s are located in close range to the other dorsolateral neurons and in most cases, all LN$_d$s together form a distinct cluster. Therefore, the cell bodies of the two neurons are located in the rLHla as well, like the previously described ITP expressing LN$_d$. The sNPF expressing cells also initially project medial, encompassing the AOT and then turn dorsal to run on the surface of the LH to the posterior side of the brain (Figure 6d). On the posterior surface, the initial branch bifurcates at the dorsal boundary between the LH and the SLP.

One branch descends toward, but does not innervate the ipsilateral AME (ventral branch, Figure 6, lower panel). It projects along the

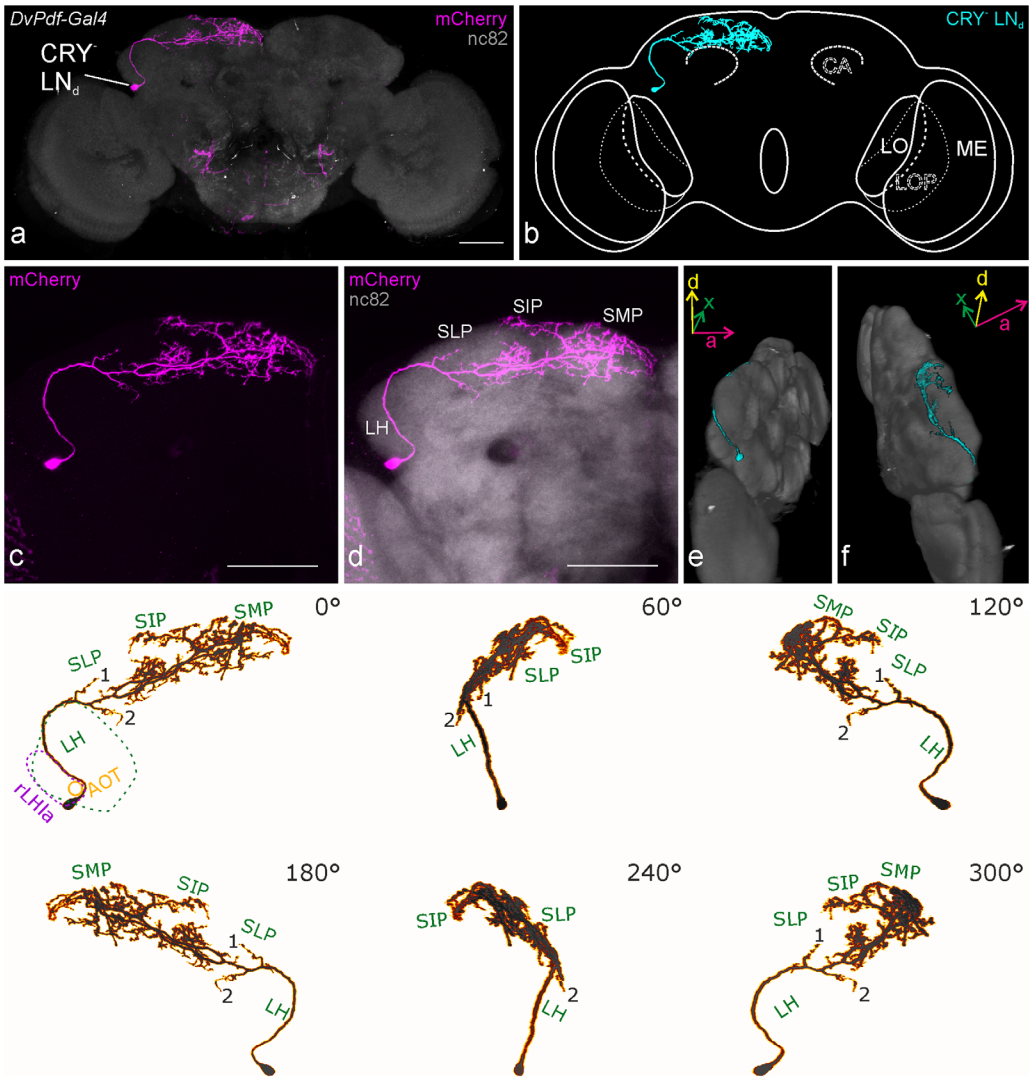

FIGURE 7 Neuroanatomy of the three CRY-negative LN_ds. (a) Exemplary overview of one of the three CRY^- LN_ds, labeled with an antisera against mCherry (magenta) and costained for the neuropils with nc82 (gray). (b) Scheme of a CRY^- LN_d. (c, d) Magnification. (e, f) Anterior-lateral (e) and posterior-lateral (f) view. Projection pattern rotated and viewed from different angles in 60° steps (lower panel). Characteristic branches are numbered for further description in the maintext and landmark fiber bundles are implied in orange (AOT). Neuropil structures are shown in dark green and the location of the cell body is highlighted in purple (rLHla). The projections do not cross the dorsoventral midline and are restricted to the ipsilateral brain hemisphere (see also a and d). a, anterior; d, dorsal; x, lateral axis. AOT, anterior optic tract; ME, medulla; LO, lobula; LOP, lobula plate; CA, calyx; PLP, posterior lateral protocerebrum; LH, lateral horn; SLP, superior lateral protocerebrum; SIP, superior intermediate protocerebrum; SMP, superior medial protocerebrum; MDC, middle dorsal commissure; SMP, superior medial protocerebrum of the contralateral hemisphere; rLHla, cell body rind lateroanterior to the lateral horn. Scale bars = 50 μm

lateral edge of the PLP, terminating in close vicinity to the PLP-LOF. On its way ventral, the fiber sends three fine projections to more medially located areas.

The first branch (1, Figure 6, lower panel) separates from the ventral branch on the posterior surface of the dorsal LH and terminates close to the dorsal main branch, after running through the LH.

The other two medial projections (2, 3, Figure 6, lower panel) branch off from the ventral fiber at the dorsoventral level of the PED and invade the posterior ventrolateral LH and posterior dorsolateral PLP.

The main projection in the dorsal brain trifurcates on the posterior surface of the lateral SLP shortly after the initial branching. The thinner side branch (4 in Figure 6, lower panel) runs anteriorly on the surface of the SLP and passes into the anterior optic tubercle (AOTU).

Most projections remain in the dorsal part of the central brain (Figure 6a). After the trifurcation of the dorsal main branch, the two thicker main branches run in parallel toward the dorsoventral midline. The more ventrally proceeding projection vastly branches in the SLP and SMP with most varicose terminals located at the ipsilateral, medial border of the SMP. This branch does not pass into the contralateral hemisphere. One projection branches off in the SLP and runs through the SCL into the SMP, also terminating very close to the medial border of the ipsilateral SMP (5 in Figure 6, lower panel).

TABLE 3 Innervation pattern of the E-cells

Neuropil/ Neuron	ME	AME	PLP	LH	SCL	ICL	AOTU	SLP	SIP	SMP	MDC	SMP'	SIP'	SLP'
sNPF$^+$ LN$_d$ (n=17)	-	-	++	+++	++	-	+++	+++	++	+++	+	+++	-	-
ITP$^+$ LN$_d$ (n=12)	+	+++	+++	++	+	++	-	+++	-	+++	+	+++	-	+
5th s-LN$_v$ (n=8)	++	+++	+++	++	+	+	-	+	-	++	+	++	-	+
CRY$^-$ LN$_d$ (n=30)	-	-	-	+	-	-	-	++	++	+++	-	-	-	-

Abbreviations were used as previously described. Commissures are highlighted in gray. n = number of individually labeled cells for analysis. + non-branching projections, ++ bifurcating projections, +++ vastly branching projections.

Another side branch of the ventrally proceeding dorsal main projection separates in the lateral SMP and projects anteriorly and laterally to reach into the dorsomedial part of the SIP (6 in Figure 6, lower panel).

The more dorsally located main fiber hardly branches in the ipsilateral hemisphere, but crosses the dorsoventral midline via the MDC and innervates the medial and center part of the contralateral SMP (Figure 6d).

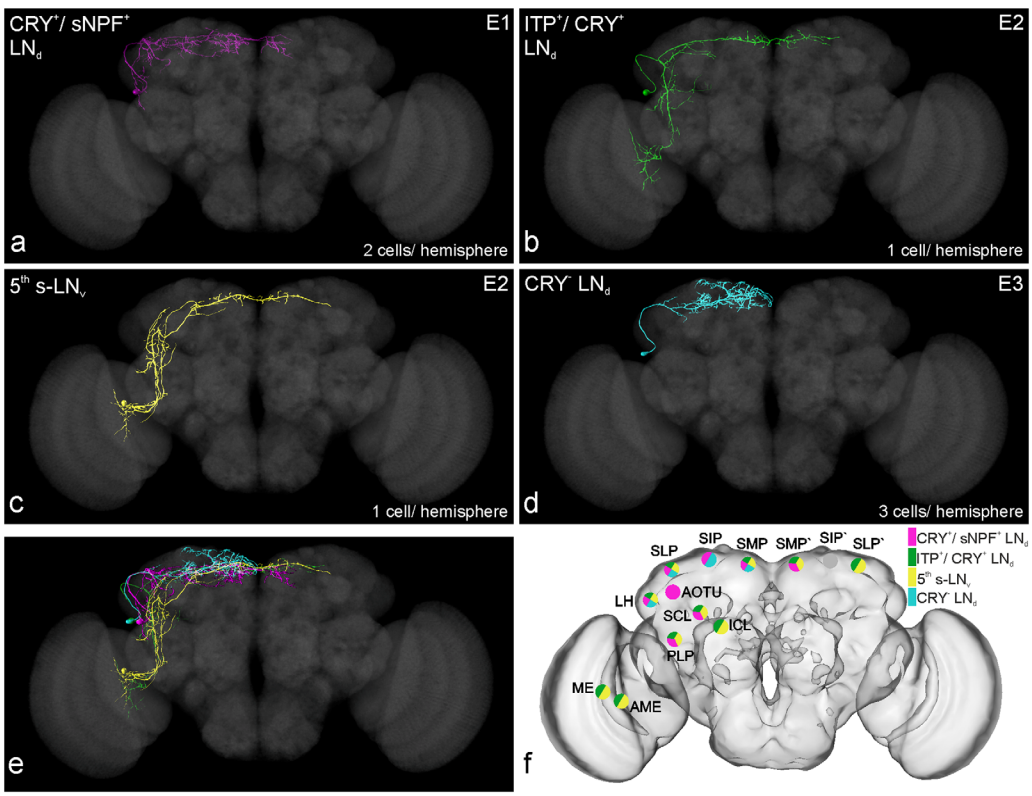

FIGURE 8 Reconstructions of representative single cell projections registered to the Janelia Farm standard brain (Jenett et al., 2012) and innervation map. Neuronal subgroups that build different E-oscillator subunits either show the same (E1 and E3) or highly comparable innervation patterns, even though they belong to different clock neuron subgroups, like the neurons of E2. (a–d) Exemplary reconstructions of the single cell projection patterns of the lateral clock neurons that comprise the E-oscillator. (a) Two LN$_d$s per brain hemisphere express the circadian photoreceptor Cryptochrome (CRY) and the short neuropeptide F (sNPF). The two neurons comprise the E1-oscillator subunit and are not distinguishable from each other in respect to their morphology or neurochemical content. (b, c) The E2-oscillator is built by two neurons that belong to different clock neuron subclusters, and their cell bodies are located in discrete areas of the brain. The LN$_d$ and the 5th s-LN$_v$ both co-express CRY and ITP and show a similar innervation pattern (see f), although they belong to different neuronal subgroups (ventrolateral neurons and dorsolateral neurons, respectively). There is only one cell of each of those neurons per brain hemisphere. (d) The E3-oscillator subunit consists of three CRY$^-$ LN$_d$s per brain hemisphere that are morphologically equal. The only criteria for discrimination is the expression of neuropeptide F (NPF) by two of the three E3 cells (Johard et al., 2009). (e) Superposition of single E-cell subtypes onto the Janelia Farm standard brain. (f) Innervation map based on the projection pattern of individually analyzed lateral clock neurons (see Table 3). ME, medulla; AME, accessory medulla; PLP, posterior lateral protocerebrum; ICL, inferior clamp; SCL, superior clamp; AOTU, anterior optic tubercle; LH, lateral horn; SLP, superior lateral protocerebrum; SIP, superior intermediate protocerebrum; SMP, superior medial protocerebrum; SMP, contralateral SMP; SIP, contralateral SIP; SLP, contralateral SLP

3.2.5 | The morphology of the three CRY lacking LN_ds

The projection pattern of the CRY absent LN_ds was analyzed by using the Flybow2.0B reporter in combination with the *DvPdf-G4* driver, which includes all three CRY lacking cells (see Figure 2b). This combination provided 30 individually labeled non-CRY LN_ds and a total of 56 neurons for analysis (individually labeled cells and sparsely labeled brains).

The cell bodies of these neurons cluster with the other LN_ds, situated dorsally to the AVLP in the rLHla (Figure 7, upper panel). The initial projection runs around the AOT and proceeds dorsally on the anterior surface of the LH (Figure 7, lower panel). It grows along the surface of the LH to the posterior side of the brain, where it turns medially to run into the superior neuropils (Figure 7).

The first side branch (1, Figure 7, lower panel) leaves the main projection at the posterior dorsolateral edge of the SLP and runs into the same neuropil. The second side branch (2, Figure 7, lower panel) separates from the main branch slightly more posterior and medial as compared to the first. This fiber projects along the posterior boundary between the LH and the SLP, terminating very close to the MB calyx (Ca).

The main tract bifurcates on the posterior surface of the SLP and continues in two fibers that run in parallel toward the dorsoventral midline (Figure 7d). The dorsal fiber does not ramify before it reaches into the SMP. Most of its branching occurs in the medial ipsilateral SMP, close to the dorsoventral border of the two hemispheres.

The more ventrally located main projection already starts to branch in the SLP, but most of the ramifications can be observed in the SMP (Figure 7d). Additionally, one projection separates from the ventral main branch in the SMP, turns laterally, and runs anterior into the dorsal SIP (Figure 7).

The CRY lacking LN_ds are the only cells of the dorsolateral clock neuron cluster that do not cross the dorsoventral midline to pass into the contralateral brain hemisphere (Figure 7a).

3.3 | Relation of the lateral clock neurons that comprise the E-oscillator

The innervation pattern of each individually labeled neuron was described by reference to the nc82 neuropil staining (see Table 3). After analyzing the projection pattern of the E-cells, the most representatives were registered to the Janelia Farm standard brain model (Jenett et al., 2012; see Figure 8) to make them comparable to available data from other sources. Besides the individually labeled neurons, we obtained numerous brains where more than one cell was tagged by a particular fluorescence protein. These brains confirmed the results from the single cell registrations to the template brain and further allowed us to analyze the relation of the single clock cells in their native coordinate space.

The cells that form an oscillator subunit (E1–E3, see introduction) also show a similar projection pattern. Only the E2 subunit consists of neurons that are morphologically distinguishable from each other, mainly due to the location of their somata and in part because of single characteristic projections (Figure 4c, i). The overall innervation pattern of the two E2 cells only differs in the innervation of the ICL (Figure 8f).

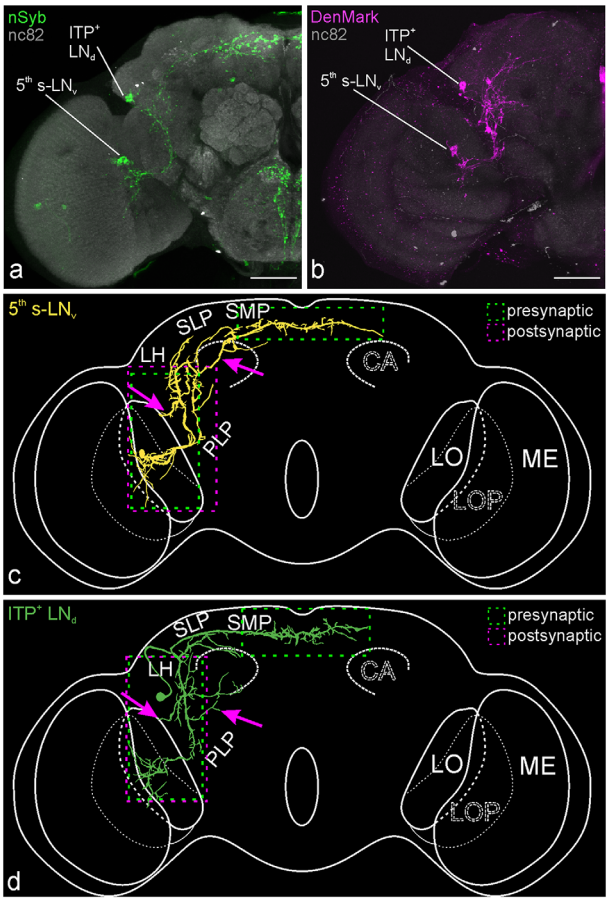

FIGURE 9 Post- and presynaptic sites of the ITP expressing LN_d together with the 5th s-LN_v. (a) *UAS-nSyb* expression (green) of *R54D11-G4/pdf-G80* brains shows putatively presynaptic sites and (b) *UAS-DenMark* (magenta) driven by the same *Gal4/Gal80* combination reveals the postsynaptic projections of the ITP^+ LN_d and the 5th s-LN_v. (c, d) Schematic overview of the 5th s-LNv's (c) and the ITP^+ LN_d's (d) polarity with presynaptic sites in green and postsynaptic sites in magenta. The fascicle which runs from the posterior lateral protocerebrum (PLP) to the lobula (LO) was exclusively labeled with the postsynaptic marker (left arrow in both overviews). Both cells possess characteristic postsynaptic fibers that are only present in the respective cell type (right arrow in both overviews). ITP, ion transport peptide; LH, lateral horn; SLP, superior lateral protocerebrum; SMP, superior medial protocerebrum; CA, calyx; LOP, lobula plate; ME, medulla. Scale bars = 50 μm

On the contrary, the remaining two E-oscillator units are comprised of cells from the same neuronal subgroup (CRY^+ or CRY^- LN_ds), which are identical within their respective oscillator subunit. All CRY expressing lateral E-cells are highly overlapping in the PLP and in the superior neuropils also with the CRY lacking LN_ds (Figure 8e). The ITP expressing cells furthermore coinvade the AME with closely related fibers.

3.4 | Identification of putative input and output sites of lateral clock neurons

After the single cell characterization of the lateral clock neurons' morphology, we went on to use the obtained knowledge to identify

putative input and output sites. In order to label the pre- and postsynaptic projections, three different reporter lines were employed. The UAS-DenMark (Nicolaï et al., 2010) is a dendritic marker (ICAM5/Telencephalin) tagged with the red fluorescence protein mCherry and specifically labels the somatodendritic compartment. For unravelling putative input sites, we used a presynaptic vesicle marker tagged with EGFP (UAS-nSyb::EGFP, neuronal Synaptobrevin::EGFP; Zhang et al., 2002). For each condition, 10 brains were analyzed.

3.4.1 | The ITP expressing cells

Reporter expression with *R54D11-G4/pdf-G80* was only found in neurons of interest (ITP$^+$ LN$_d$ and 5th s-LN$_v$) and in the subesophageal zone, belonging to non-clock neurons (Figure 2e). Due to the vast overlap of the projections stemming from the ITP expressing LN$_d$ and the 5th s-LN$_v$, separation and assignment of the single projections was only possible in respect to the single-cell data and by going through the confocal stacks slice by slice. The nature of nSyb labeling hampered the segmentation and the assignment of the signal to specific projections, nevertheless, we were able to track some neurites from their origin at the cell body until they reach the superior neuropils. The two E2 cells presumably possess presynaptic sites in the AME and on the extensions reaching into the M7 margin of the ME (Figure 9c, d). We observed weak GFP expression in the PLP, most likely from neurites of both, 5th s-LN$_v$ and the ITP producing LN$_d$. Almost no presynaptic vesicle marker was expressed in the lateral and intermediate superior neuropils, but strong labeling occurred in the SMP, where the projections of both hemispheres are vastly overlapping (Figure 9a).

Interpreting the signal from the Telencephalin::mCherry (TLN, DenMark) reporter in *R54D11-G4* brains was easier, since we could easily follow the projections with reference to the single cell morphological data. The addressed clock neurons (5th s-LN$_v$ and LN$_d$) both have postsynaptic terminals in the AME, although there are fewer fibers labeled as compared to the nSyb::GFP (Figure 9a, b). In the PLP and the SCL postsynaptic sites could be identified originating from both neuron types. The projections of the two neurons that contribute to the PLP-LOF could only be seen with the DenMark reporter, but not with nSyb::GFP (Figure 9a, b, left arrow in c, d). The postsynaptic neurites in the dorsolateral part of the brain could be allocated to the 5th s-LN$_v$ (indicated by the upper right arrow in Figure 9d).

3.4.2 | The sNPF expressing LN$_d$s

With the *R16C05-G4* driver line and *UAS*-nSyb::EGFP only the presynaptic vesicles of two DN$_{1a}$ and the two sNPF/CRY coexpressing LN$_d$s were labeled (Figure 10a). The single-cell studies helped to disentangle and assign the projections of the different neurons labeled by the synaptic markers. In the two LN$_d$s, the tagged presynaptic protein was found in the somata and in the initial projection running around the LH (Figure 10a). We observed weak expression in the projections in the

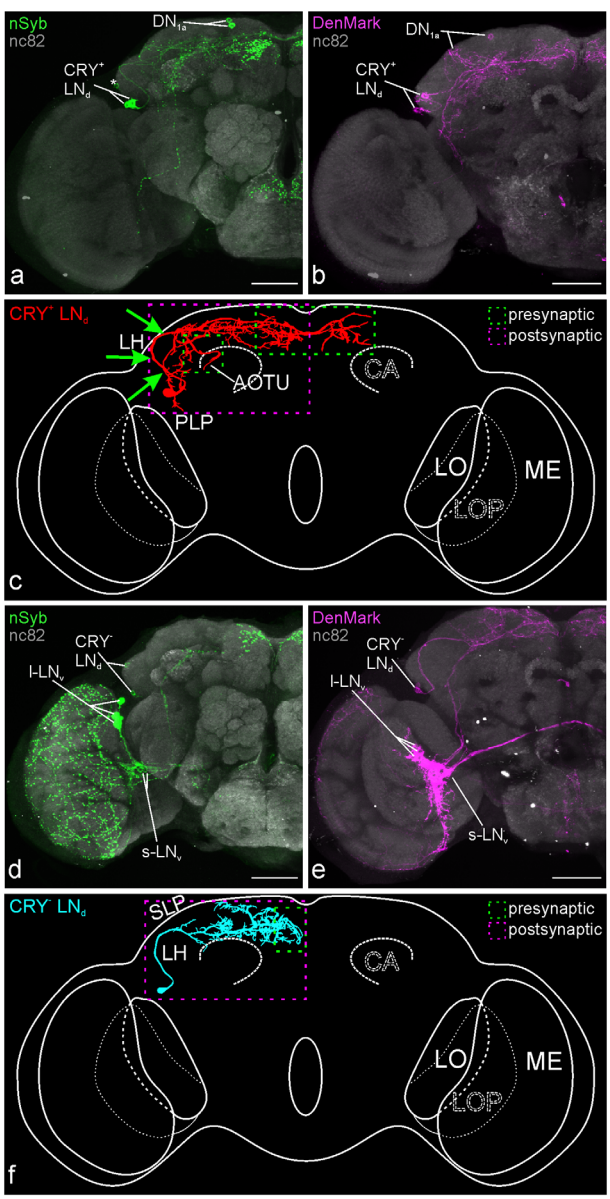

FIGURE 10 Post- and presynaptic sites of the ITP-negative LN$_d$s. (a) Expression of *R16C05-G4/UAS-nSyb* (green) to reveal putative presynaptic arborizations of the CRY$^+$ LN$_d$s together with the DN$_{1a}$. (b) *R16C05-G4/UAS-DenMark* expression (magenta) in the postsynaptic branches of the CRY$^+$ LN$_d$s and the DN$_{1a}$. The soma of a non-clock cell can be seen at the lateral edge of the lateral horn (asterisk), but the marker expression in the neurites was too weak to interfere with the identification of clock cell projections. (c) Schematic overview of the polarity of CRY$^+$ LN$_d$s with postsynaptic sites in magenta and presynaptic sites in green. The projection on the surface of the lateral horn (LH) expressed the presynaptic marker (green arrows), but the majority of the arborizations in the ipsilateral superior brain regions could only be seen with the postsynaptic marker. (d–f) Post- and presynaptic sites of the CRY$^-$ LN$_d$s. (d) *UAS-nSyb* (green) expression shows putative presynaptic sites in the brains of *DvPdf-G4/cry-G80* flies and (e) *UAS-DenMark* (magenta) revealed the postsynaptic arborizations. *Cry-G80* did not sufficiently suppress the reporter expression in the PDF$^+$ LN$_v$s, but worked in the ITP$^+$ LNd and the 5th s-LN$_v$. (f) Schematic overview of the post- and presynaptic sites of the CRY$^-$ LN$_d$s in magenta and green, respectively. CRY, cryptochrome; PLP, posterior lateral protocerebrum; AOTU, anterior optic tubercle; SLP, superior lateral protocerebrum; CA, calyx; LO, lobula; LOP, lobula plate; ME, medulla. All scale bars = 50 μm

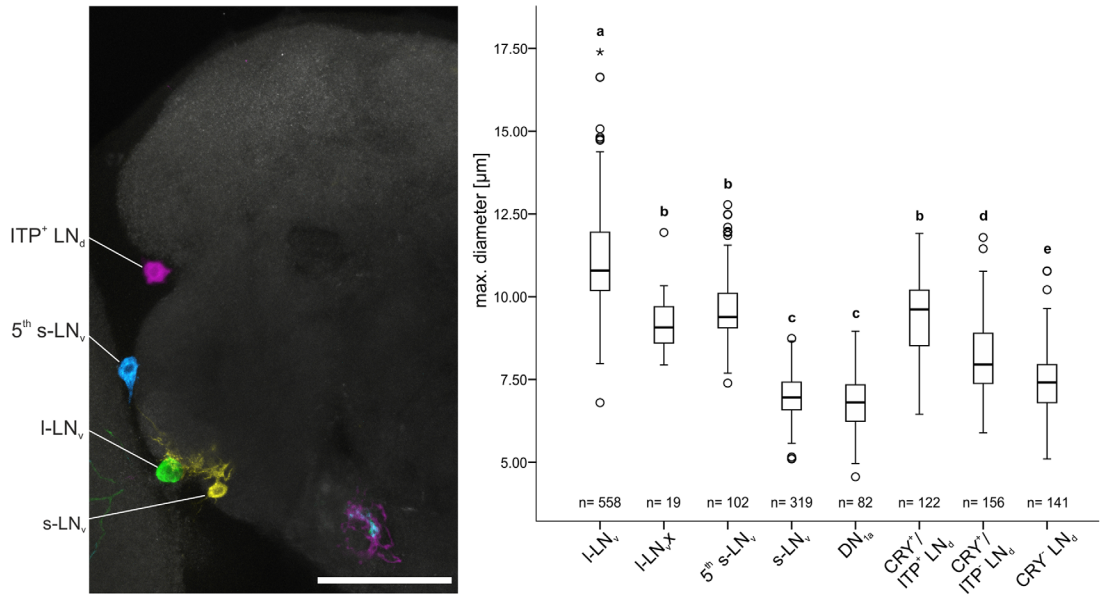

FIGURE 11 Comparison of the estimated cell diameters of clock neurons. A one way ANOVA with post hoc Bonferroni correction was performed for statistical testing. Contrary to the current nomenclature the 5th s-LN_v shows the third largest cell diameter, surpassed in size only by the l-LN_vs and the ITP^+ LN_d (not significant) and it is significantly larger than the PDF^+ s-LN_vs. Significant differences are indicated with different letters. The same letter means that there was no statistical disparity in cell diameter between the cell types. All indicated differences were highly significant with $p < .01$. CRY, cryptochrome; ITP, ion transport peptide. Scale bar = 50 µm

SLP and PLP, but more strongly labeled vesicles in the AOTU (Figure 10a). The strongest labeling with nSyb::EGFP occurred in the terminals in the SMP, where the projections of the LN_ds of both hemispheres overlap (Figure 10a). Note that the fibers, running through the MDC and connecting both hemispheres, are also putatively presynaptic (Figure 10a). The signal posterior to the AOTU, close to the mushroom body CA, and the fiber running through the PLP into the AME belongs to the DN_{1a} in the dorsal brain (Figure 10a). Labeling in the subesophageal zone belongs to non-clock neurons (see Figure 2a).

The postsynaptic reporter TLN::mCherry was localized in the complete ipsilateral projections of the sNPF and CRY expressing LN_ds (Figure 10b), indicating that some sites are pre- and postsynaptic. We observed strong reporter expression in the somata and even labeling of the somatodendritic compartment. The sNPF/CRY producing LN_ds' postsynaptic projections can be seen in the PLP, LH and in the superior neuropils, as well as in the fiber that runs anteriorly into the SLP (Figure 10b). Notably, there was no reporter signal in the MDC, suggesting that these cells have postsynaptic sites only ipsilateral (Figure 10b).

3.4.3 | The CRY lacking LN_ds

In order to analyze the putative in- and output-sites of the CRY lacking LN_ds, we crossed the *DvPdf-G4* driver to the respective reporters and utilized the *Gal4*-repressor *cry-G80*, hoping to restrict the reporter expression only to those cells in which CRY is absent. Unfortunately, we found that the *cry-G80* construct does not sufficiently suppress the reporter expression in the PDF-cells (as reported in Guo et al., 2014). However, *Gal4* repression worked for the remaining CRY expressing LNs (5th s-LN_v and ITP^+ LN_d), which would otherwise impede the analysis due to the vast overlap of their projections. The presynaptic vesicle marker labeled the cytoplasm of the three LN_ds without CRY expression, as well as their terminals in the SMP close to the dorsoventral midline (Figure 10d, f). In contrast to the presynaptic marker, labeling with the TLN::mCherry occurred over the entire neuronal structure, suggesting that they get input from various dorsal clock neurons, which are branching in the superior neuropils (Figure 10e, f).

3.5 | Comparison of estimated cell diameters

For the simple reason that nine out of 15 lateral clock neurons are not only named due to their location in the brain, but also after the relative size of their soma (s-LN_vs, l-LN_vs, and 5th s-LN_v), we ascertained the maximal cell diameter of individually labeled clock neurons and compared them to each other (see Figure 11). Surprisingly, we found that the 5th s-LN_v is considerably larger compared to the remaining, PDF expressing s-LN_vs (9.60 ± 0.88 µm to 7.01 ± 0.66 µm, see Figure 11). However, it was very interesting to see, that the 5th s-LN_v and the ITP expressing LN_d, which are a functional unit, have comparable cell diameters (9.60 ± 0.88 µm and 9.44 ± 1.11 µm, respectively). Solely the l-LN_vs have been found to be significantly larger as the 5th s-LN_v (11.07 ± 1.42 µm to 9.60 ± 0.88 µm). On the other side there was no statistical difference in cell diameters between the 5th s-LN_v and the newly described l-LN_vx (9.60 ± 0.88 µm to 9.31 ± 0.88 µm). The PDF producing s-LN_vs fall in line with the dorsal neurons in the anterior brain (DN_{1a}; 7.01 ± 0.66 µm and 6.76 ± 0.88 µm, respectively). The analysis of the cell diameters again substantiates the heterogeneity of the dorsolateral clock neurons. Each subtype of LN_ds is showing a significantly different cell diameter (ITP^+ LN_d: 9.44 ± 1.11 µm; CRY^+ LN_ds: 8.15 ± 1.14 µm; CRY^- LN_ds: 7.52 ± 0.97 µm).

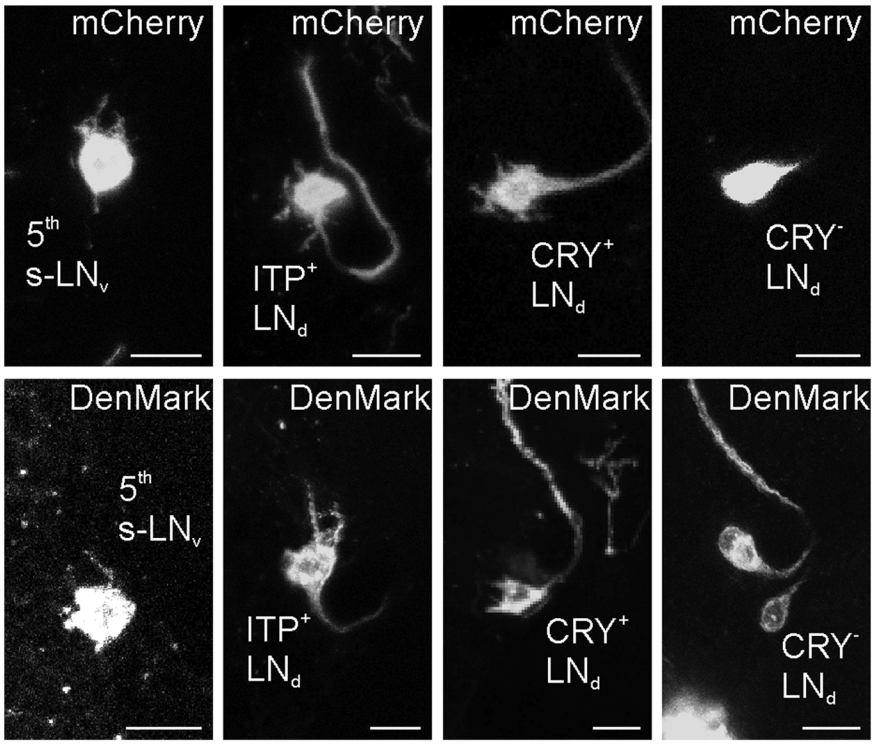

FIGURE 12 Comparison of the soma morphology of the E-cells. In contrast to the CRY$^-$ LN$_d$s, the somata of all the CRY expressing E-cells possess small membrane-appendages. The same appendages can be seen with *DenMark* expression, suggesting that these varicosities are likely postsynaptic. CRY, cryptochrome; ITP, ion transport peptide. Scale bars = 10 μm

While comparing the estimated cell sizes we noticed that particular cell types had membrane appendages at their cell bodies (Figure 12 upper row). These membrane outgrowths were restricted to the CRY expressing E-cells and were consistently labeled with the DenMark reporter (Figure 12). The smaller CRY$^-$ LN$_d$s had rather smooth somata surfaces (Figure 12).

4 | DISCUSSION

We conducted the current study with respect to three central questions. First and foremost we wanted to scrutinize the morphological characteristics and differences of the single neurons within the subgroups of LNs particularly with regard to the cells that comprise the E-oscillator (i.e., 5th s-LN$_v$s, CRY$^+$ LN$_d$s, and CRY$^-$ LN$_d$s). The second object of research was to comment on the assumed innervation of the AME by all CRY expressing LN$_d$s, based on the lack of means in earlier studies to reliably dissect the overlapping neurites of individual cells. The final aim was to provide a complementary overview of putative post- and presynaptic sites of the LNs to identify candidate regions where downstream neurons of the clock might be located nearby, and where clock neurons might be in direct contact to each other.

4.1 | The l-LN$_v$s are a heterogenic group of clock neurons with distinct arborization patterns

The classification of the l-LN$_v$s as M-oscillators is a controversely discussed fact (e.g., Beuchle, Jaumouille, & Nagoshi, 2012; Abruzzi, Chen, Nagoshi, Zadina, & Rosbash, 2015). Though, the release of high levels of PDF which acts directly on E-cells to control the phasing of the evening activity peak independently from s-LN$_v$ signaling (Cusumano et al., 2009; Potdar & Sheeba, 2012; Schlichting et al., 2016), as well as the described role of l-LN$_v$s in the control of sleep and arousal (Parisky et al., 2008; Sheeba, Gu, Sharma, O'Dowd, & Holmes, 2008; Gmeiner et al., 2013) justifies this assumption.

By utilizing the Flybow multicolor technique we could demonstrate for the first time that the current subdivision of M-cells into s- and l-LN$_v$s is too simplified and we introduced the term l-LN$_v$x for a newly described morphological subclass of l-LN$_v$s. Our results indicate that there is only one l-LN$_v$x opposing to three regular l-LN$_v$s per brain hemisphere. Either l-LN$_v$ subtype shows a similar initial branching pattern, which has already been described by Park and Griffith (2006) based on fluorescence dye-fills. The small number of backfilled neurons in their study, however, could not reveal the presence of the l-LN$_v$x and our approach, using membrane targeted fluorescence proteins is considerably superior in order to expose the neuronal structure in its entirety. Likewise we report first that l-LN$_v$ and l-LN$_v$x projections, originating from the primary ventral branch, are extensively invading the serpentine layer of the ipsilateral ME and that these projections colocalize with fibers from the ITP-expressing E-cells (5th s-LN$_v$ and one LN$_d$). The E-cell-, as well as the l-LN$_v$ neurites in this region were responsive to n-Syb and DenMark labeling, supporting the findings of Schlichting et al. (2016), who were the first to demonstrate a direct functional link between the l-LN$_v$s and the E-cells in the adjacently located AME. In the same study, the authors conclude that l-LN$_v$ PDF-

signaling to the NPF and ITP expressing E-cells gets more important for proper timing of the E-activity peak with increasing day lengths, suggesting a functional relevant disparity between s- and l-LN_v secreted PDF (Schlichting et al., 2016). Hence they provided evidence for an important link between the neurons that our study focused on (l-LN_vs and E-cells).

Due to the shared initial branching and projection pattern, both l-LN_v subclasses contribute to the ipsilateral AME_{vel}, even though the individual l-LN_vs project further along the ventral edge to the posterior side and thereby proceed toward the distal ME more often. The strikingly different projection pattern on the surface of the ipsi- and contralateral ME is the more apparent disparity. The regular l-LN_vs project in the accustomed manner (Helfrich-Förster et al., 2007), forming a network that covers the surface of the ME of both hemispheres. As already described by Helfrich-Förster et al. (2007), the main target area of the l-LN_vs is the distal ME, where the fibers are densely running along the lateral edge. In contrast, the outstanding l-LN_vx exclusively invades the dorsomedial and ventromedial surface of the ME, indicating that these cells might have a unique function among the l-LN_vs. This indication strengthens the necessity of anatomical single cell studies to provide valuable reference to push our understanding of complex neuronal networks, not only on the anatomical, but also on the functional level.

4.2 | The E-oscillator can be subdivided according to their morphology and function

Thanks to the widely utilized antibody against synthetic β-PDH, the anatomy of the PDF expressing LN_vs could be described early on and they were the first clock neurons in *Drosophila* with a revealed projection pattern (Helfrich-Förster & Homberg, 1993). In contrast, the morphology of the LN_ds remained elusive for more than one additional decade, until Helfrich-Förster and her colleagues provided the first decent description of *Drosophila*'s clock network (Helfrich-Förster et al., 2007; Yoshii et al., 2008; Johard et al., 2009). Whether the CRY expressing LN_ds make contact with other clock neurons in the AME is a central question that remained unanswered by previous studies and therefore was one of our main interests. We furthermore endeavored to clarify of potential refined morphological differences among the CRY expressing LN_ds, according to the different functions they are attributed with (Rieger et al., 2006; Shafer et al., 2006; Yao & Shafer, 2014).

Our study is the first, demonstrating that the functional subdivision of the LN_ds is reflected in their morphology. The projections of the two ITP lacking, CRY producing LN_ds (those are the sNPF expressing LN_ds, Johard et al., 2009), that are strongly coupled to the s-LN_v output via PDFR signaling (Yao & Shafer, 2014), do not reach far enough ventrally to possibly invade the AME and make direct contact with other clock cells there. Our results are further indicating that there is no structural difference between the two sNPF expressing cells.

According to the current working model of peptidergic unit composition of *Drosophila*'s clock, the ITP expressing LN_d is assigned to another oscillator unit (E2), which also includes the 5th s-LN_v. The two ITP expressing clock neurons have never been shown separately before and we were surprised by their remarkable resemblance as it was generally assumed that the 5th s-LN_v would look like the PDF containing s-LN_vs. Instead, the ITP clock cells show an almost identical projection pattern, reflecting their functional similarity. Our detailed study clearly demonstrates that out of all LN_ds, solely the ITP expressing one is invading the AME. Among the E-cells, innervation of the AME is an exclusive feature of the E2 subunit.

For the CRY lacking LN_ds it has already been assumed that they would not project ventrally toward the AME. However, with the current study we showed for the first time that (a) the CRY lacking LN_ds' projections are indeed restricted to the superior neuropils only, (b) there is no systematic morphological difference between those neurons and (c) these are the only E-cells that do not cross the dorsoventral midline into the contralateral hemisphere.

Overall, this is the first work providing clear evidence for a morphological subdivision of the E-oscillator that is in line with the already described functional subunits.

4.3 | The 5th s-LN_v: a LN_d in disguise

Although the 5th s-LN_v has always stood out from the other s-LN_vs, as it is the only one without PDF expression, it has been assumed that all s-LN_vs share a similar projection pattern. This assumption has now proven to be false and the soma size on its own already discriminates the 5th from the other s-LN_vs. In the previous parts, we already discussed morphological and functional similarities of the 5th s-LN_v and the ITP expressing LN_d, once more raising the question whether the 5th s-LN_v might in fact belong to the LN_ds rather than to the s-LN_vs.

In conclusion, neurochemical content (Helfrich-Förster, 1995; Kaneko, Helfrich-Förster, & Hall, 1997), observed function (Rieger et al., 2006; Im, Li, & Taghert, 2011; Yao & Shafer, 2014), as well as developmental studies (Helfrich-Förster et al., 2007; Liu, Mahesh, Houl, & Hardin, 2015) already argue against classifying the 5th LN_v as a s-LN_v, since this might imply similarities with the PDF expressing cells. So far, it has been assumed that the 5th s-LN_v would at least have the same projection pattern as the remaining PDF containing s-LN_vs, justifying the nomenclature despite all this. However, the findings of our study, which revealed the morphological differences of the 5th s-LN_v to the PDF cells on one hand, and the striking similarities with the ITP expressing LN_d on the other, opens the discussion whether the nomenclature of the 5th s-LN_v is still applicable. This becomes even more questionable with respect to the measurements of the clock neuron somata sizes. We demonstrated that, once again, the 5th s-LN_v is more comparable to the ITP expressing LN_d and significantly larger than the s-LN_vs. Actually, the 5th s-LN_v is on average the same size as the l-LN_vx and only slightly smaller than the other l-LN_vs. This means even the relative cell size of the 5th s-LN_v argues against naming it "small." In terms of classical nomenclature, which referred to the size and location of the cell body, the 5th s-LN_v would have to be called "5th l-LN_v" correctly. This, however, would be as misleading as the current nomenclature. To nonetheless emphasize the unique character of the 5th s-LN_v and to differentiate them from the other LN_vs, we propose to refer

to this neuron as the "5th LN_v", since this would correctly name the location without implying any further commonalities with other LN_vs. The designation "5th" would still be correct in various respects, as it is one of the five early LN_v pacemaker neurons. As there are four l-LN_vs and four s-LN_vs, it would still be the "5th" neuron, regardless of which cluster it would have theoretically been assigned to.

4.4 | The network and its putative connections

Even before this study, it has been well established that the clock neurons form a vastly overlapping network (Helfrich-Förster, 2003; Helfrich-Förster et al., 2007), which integrates multisensory inputs (e.g., light and temperature cues) from the environment (Helfrich-Förster et al., 2002; Yoshii, Sakamoto, & Tomioka, 2002; Yoshii et al., 2005; Busza, Murad, & Emery, 2007; Yoshii et al., 2008; Veleri, Rieger, Helfrich-Förster, & Stanewsky, 2007; Picot, Klarsfeld, Chélot, Malpel, & Rouyer, 2009; Sehadova et al., 2009; Yoshii, Vanin, Costa, & Helfrich-Förster, 2009; Kaneko et al., 2012; Buhl et al., 2016; Harper, Dayan, Albert, & Stanewsky, 2016; Tang et al., 2017). Although *Drosophila*'s clock has been shown to have an implication on the fly's metabolism (Xu, Zheng, & Sehgal, 2008; Xu, DiAngelo, Hughes, Hogenesch, & Sehgal, 2011), sleep (Hendricks et al., 2000; Shaw, Cirelli, Greenspan, & Tononi, 2000; Hendricks et al., 2003), the control of locomotor rhythms (Konopka & Benzer, 1971; Handler & Konopka, 1979; Helfrich & Engelmann, 1983), the gating of eclosion and metamorphosis (Pittendrigh & Skopik, 1970; Konopka & Benzer, 1971; Hamblen-Coyle, Wheeler, Rutila, Rosbash, & Hall, 1992; Sehgal, Price, Man, & Young, 1994; Myers, Yu, & Sehgal, 2003), as well as on learning and memory (Lyons & Roman, 2009; Fropf et al., 2014; Chouhan, Wolf, Helfrich-Förster, & Heisenberg, 2015), the coverage of specific connections to downstream neurons of the circadian network still lags behind. So far, only six studies have been able to identify specific target neurons, reporting their implication in the control of rest:activity- (Pírez, Christmann, & Griffith, 2013; Cavanaugh et al., 2014) and wakefulness:sleep-cycles (Cavanaugh, Vigderman, Dean, Garbe, & Sehgal, 2016; Cavey, Collins, & Blau, 2016; King et al., 2017), metabolic regulation (Barber, Erion, Holmes, & Sehgal, 2016), and the coupling of the peripheral clock of prothoracic gland (PG) to the central pacemaker in the brain (Selcho et al., 2017). In the upcoming years, the research focus will increasingly shift from the already well-described input pathways and clock network properties to the outputs and its underlying circuits.

We identified several neuropils, in which clock neuron projections went so far unnoticed or have not been analyzed in great detail (SCL, ICL, AOTU, ME serpentine layer). These neuropils are candidate regions for the possible localization of downstream neurons or their arborizations, which has to be investigated more closely.

The clamp (SCL and ICL) contains fibers of the two ITP expressing clock cells (LN_d and 5th s-LN_v). Additionally, the posteriorly located neuropil gets densely innervated by fibers, stemming from *fruitless* and *doublesex* expressing neurons, which belong to the courtship circuit (Cachero, Ostrovsky, Yu, Dickson, & Jefferis, 2010; Rideout, Dornan, Neville, Eadie, & Goodwin, 2010; Robinett, Vaughan, Knapp, & Baker, 2010; Yu, Kanai, Demir, Jefferis, & Dickson, 2010; Zhou et al., 2015). Courtship and mating behavior is controlled by the circadian clock and depends on the expression of the clock genes (Sakai & Ishida, 2001; Tauber, Roe, Costa, Hennessy, & Kyriacou, 2003; Manoli et al., 2005; Fujii, Krishnan, Hardin, & Amrein, 2007). Since the increased evening locomotor activity correlates with reduced courtship and mating frequency (Sakai & Ishida, 2001; Fujii et al., 2007), it is conceivable that the E-cells might signal onto the courtship neurons in the clamp.

The *fruitless* expressing courtship neurons additionally arborize into the AOTU (Manoli et al., 2005), a neuropil, in which projections from the clock neurons have not yet been reported. With the help of membrane targeted 10-fold reporters, we provide evidence that clock neuron subgroups ($sNPF^+/CRY^+$ LN_ds) invade the lateralmost AOTU, suggesting yet another location where interaction between clock cells and courtship neurons are possible.

Interestingly, the optic tubercle is demonstrably an integral part of the polarization vision pathway of many insects, which enables them to navigate via sun compass orientation (reviewed by el Jundi, Pfeiffer, Heinze, & Homberg, 2014). To compensate for the changes of solar elevation and the hence resulting sensory conflicts, the sky compass requires information from the circadian clock, which might get integrated at the level of the POTU and CX in locusts, cockroaches, and honeybees (reviewed by el Jundi et al., 2014). For *Drosophila*, the insect with the best-studied circadian clock, no polarization vision pathway had been described until Omoto et al. (2017) identified the anterior visual pathway (AVP) as the underlying neural substrate. The AVP is a three-legged pathway, connecting the serpentine layer of the medulla to the lateral-most AOTU, the AOTU to the bulb, and the bulb to the ellipsoid body of the CX (Omoto et al., 2017). Strikingly, we discovered clock neuron arborizations in two out of the four structures, particularly in the serpentine layer of the ME, stemming from the l-LN_vs and ITP expressing E2-neurons (5th s-LN_v, one LN_d), and in the lateral-most AOTU, originating from the E1-neurons ($sNPF^+$ LN_ds). The mere fact that this is the only physical overlap of the circadian network with the sky compass pathway in the fly, highly recommends further examination of this observation in order to possibly reveal the functional link of the two systems.

En route for the AOTU, the clock neuron fibers run close by the dendrites of the prothoracicotropic hormone (PTTH) producing cells, which reportedly couple the central pacemaker to the PG clock (Selcho et al., 2017). A PDF independent link from the s-LN_vs to the PTTH neurons via sNPF has already been demonstrated (Selcho et al., 2017), but since the E1-neurons (2 CRY^+ LN_ds) are likewise expressing sNPF, a contribution of those cells cannot be ruled out completely.

Further, two of the initially mentioned reports specified distinct cell populations in the PI as downstream targets of the DN_{1p} (Cavanaugh et al., 2014; Barber et al., 2016; King et al., 2017), confirming a long-suspected connection (Kaneko & Hall, 2000; Helfrich-Förster, 2003; Helfrich-Förster et al., 2007). The PI is considered the *Drosophila* equivalent of the mammalian hypothalamus (de Velasco et al., 2007), housing a variety of discrete populations of neurosecretory cells (Rowell, 1976; Zaretsky & Loher, 1983; Homberg, Davis, & Hildebrand, 1991a; Homberg, Wurden, Dircksen, & Rao, 1991b; Veelaert, Schoofs, & De Loof, 1998; Siegmund & Korge, 2001; de Velasco et al., 2007). In

2014, Cavanaugh et al. identified six PI neurons and their output molecule (DH44) as an integral part of the pathway controlling rest:activity rhythms. They further noted that the DH44 expressing cells are entirely complementary to the *Drosophila* insulin-like peptide (DILP2) producing cells in the PI (Cavanaugh et al., 2014), which demonstrably contribute to the regulation of sleep and metabolism (Rulifson, Kim, & Nusse, 2002; Broughton et al., 2005; Crocker, Shahidullah, Levitan, & Sehgal, 2010). Two years later, the same group demonstrated a functional link between the DN_{1p} and DILP2 cells, which regulates rhythmic expression of metabolic genes in the fat body via DILP2 signaling (Barber et al., 2016). Our results indicate that most lateral clock neurons directly target the abovementioned or other cells of the PI, too. Except for the PDF neurons and the DN_{1a}, all clock cells possess varicose arborizations in the SMP, close by the dendrites of the PI neurons. Particularly the analysis of putative in- and output sites, showing the presynaptic nature of the E-cells' projections in that region, furthermore suggests the PI as a target of multiple clock neurons. Since the s-LN_vs (Fernández, Berni, & Ceriani, 2008; Sivachenko, Li, Abruzzi, & Rosbash, 2013; Gorostiza, Depetris-Chauvin, Frenkel, Pírez, & Ceriani, 2014; Petsakou, Sapsis, & Blau, 2015) and the DN_2 (Tang et al., 2017) are reported to undergo activity-dependent circadian remodeling, it is likely, that also other clock neurons experience neuronal circadian plasticity. We controlled this effect in our study by collecting and fixing all samples at a particular time-point (ZT23). However, to obtain the complete picture of possible innervations throughout the day, a time-series analysis is required.

In conclusion, the anatomical study with single-cell resolution not only provided new insights into the clock network, but also yielded various candidate regions in the brain where potential downstream connections to other systems might be revealed in the future.

ACKNOWLEDGMENTS

Iris Salecker for providing us with the Flybow2.0B reporter transgenes, Heinrich Dircksen for ITP antisera, Takeshi Todo for CRY antisera, Isaac Edery for TIM antisera and Irina Wenzel for language correction. This study was funded by the German Research Foundation (DFG), collaborative research center SFB 1047 "Insect timing", project A3.

AUTHOR CONTRIBUTIONS

All authors had full access to all the data in the study and take responsibility for the integrity of the data and the accuracy of the data analysis. Study concept and design: FKS, DR. Acquisition of data: FKS, NH. Analysis and interpretation of data: FKS, CHF, DR. Drafting of the manuscript: FKS, DR. Figure arrangement: FKS. Critical revision of the manuscript for important intellectual content: TY, CHF. Obtained funding: DR. Study supervision: TY, CHF, DR.

ORCID

Dirk Rieger http://orcid.org/0000-0001-5597-5858

REFERENCES

Abruzzi, K., Chen, X., Nagoshi, E., Zadina, A., & Rosbash, M. (2015). Chapter seventeen-RNA-seq profiling of small numbers of *Drosophila* neurons. *Methods in Enzymology*, *551*, 369–386.

Bahn, J. H., Lee, G., & Park, J. H. (2009). Comparative analysis of Pdf-mediated Circadian behaviors between *Drosophila melanogaster* and *D. virilis*. *Genetics*, *181*, 965–975.

Barber, A. F., Erion, R., Holmes, T. C., & Sehgal, A. (2016). Circadian and feeding cues integrate to drive rhythms of physiology in *Drosophila* insulin-producing cells. *Genes and Development*, *30*, 2596–2606.

Beuchle, D., Jaumouille, E., & Nagoshi, E. (2012). The nuclear receptor unfulfilled is required for free-running clocks in *Drosophila* pacemaker neurons. *Current Biology*, *22*, 1221–1227.

Broughton, S. J., Piper, M. D., Ikeya, T., Bass, T. M., Jacobson, J., Driege, Y., … Partridge, L. (2005). Longer lifespan, altered metabolism, and stress resistance in *Drosophila* from Ablation of cells making insulin-like ligands. *Proceedings of the National Academy of Sciences of the United States of America*, *102*, 3105–3110.

Brown, S. A., Kowalska, E., & Dallmann, R. (2012). (Re)inventing the circadian feedback loop. *Developmental Cell*, *22*, 477–487.

Buhl, E., Bradlaugh, A., Ogueta, M., Chen, K. F., Stanewsky, R., & Hodge, J. J. (2016). Quasimodo mediates daily and acute light effects on *Drosophila* clock neuron excitability. *Proceedings of the National Academy of Sciences of the United States of America*, *113*, 13486–13491.

Busza, A., Murad, A., & Emery, P. (2007). Interactions between circadian neurons control temperature synchronization of *Drosophila* behavior. *Journal of Neuroscience*, *27*, 10722–10733.

Cachero, S., Ostrovsky, A. D., Yu, J. Y., Dickson, B. J., & Jefferis, G. S. X. E. (2010). Sexual dimorphism in the fly brain. *Current Biology*, *20*, 1589–1601.

Cavanaugh, D. J., Geratowski, J. D., Wooltorton, J. R., Spaethling, J. M., Hector, C. E., Zheng, X., … Sehgal, A. (2014). Identification of a circadian output circuit for rest: Activity rhythms in *Drosophila*. *Cell*, *157*, 689–701.

Cavanaugh, D. J., Vigderman, A. S., Dean, T., Garbe, D. S., & Sehgal, A. (2016). The *Drosophila* circadian clock gates sleep through time-of-day dependent modulation of sleep-promoting neurons. *Sleep*, *39*, 345–356.

Cavey, M., Collins, B., & Blau, J. (2016). Circadian rhythms in neuronal activity propagate through output circuits. *Nature Neuroscience*, *19*, 587–595.

Chouhan, N. S., Wolf, R., Helfrich-Förster, C., & Heisenberg, M. (2015). Flies remember the time of day. *Current Biology*, *25*, 1619–1624.

Crocker, A., Shahidullah, M., Levitan, I. B., & Sehgal, A. (2010). Identification of a neural circuit that underlies the effects of octopamine on Sleep:Wake behavior. *Neuron*, *65*, 670–681.

Cusumano, P., Klarsfeld, A., Chélot, E., Picot, M., Richier, B., & Rouyer, F. (2009). Modulated visual inputs and cryptochrome define diurnal behavior in *Drosophila*. *Nature Neuroscience*, *12*, 1431–1437.

De Velasco, B., Erclik, T., Shy, D., Sclafani, J., Lipshitz, H., McInnes, R., & Hartenstein, V. (2007). Specification and development of the pars intercerebralis and pars lateralis, neuroendocrine command centers in the *Drosophila* brain. *Developmental Cell*, *302*, 309–323.

Dircksen, H., Tesfai, L. K., Albus, C., & Nässel, D. R. (2008). Ion transport peptide splice forms in central and peripheral neurons throughout postembryogenesis of *Drosophila melanogaster*. *The Journal of Comparative Neurology*, *509*, 23–41.

el Jundi, B., Pfeiffer, K., Heinze, S., & Homberg, U. (2014). Integration of polarization and chromatic cues in the insect sky compass. *Journal of Comparative Physiology*, *200*, 575–589.

Fernández, M. P., Berni, J., & Ceriani, M. F. (2008). Circadian remodeling of neuronal circuits involved in rhythmic behavior. *PLoS Biology*, *6*, e69.

Fropf, R., Zhang, J., Tanenhaus, A. K., Fropf, W. J., Siefkes, E., & Yin, J. C. (2014). Time of day influences memory formation and dCREB2 proteins in *Drosophila*. *Frontiers in Systems Neuroscience*, *8*, 1–10.

Fujii, S., Krishnan, P., Hardin, P., & Amrein, H. (2007). Nocturnal male sex drive in *Drosophila*. *Current Biology*, *17*, 244–251.

Gmeiner, F., Kołodziejczyk, A., Yoshii, T., Rieger, D., Nässel, D. R., & Helfrich-Förster, C. (2013). GABAB receptors play an essential role in maintaining sleep during the second half of the night in *Drosophila melanogaster*. *Journal of Experimental Biology*, *216*, 3837–3843.

Gorostiza, E. A., Depetris-Chauvin, A., Frenkel, L., Pírez, N., & Ceriani, M. F. (2014). Circadian pacemaker neurons change synaptic contacts across the day. *Current Biology*, *24*, 2161–2167.

Grima, B., Chélot, E., Xia, R., & Rouyer, F. (2004). Morning and evening peaks of activity rely on different clock neurons of the *Drosophila* brain. *Nature*, *431*, 869–873.

Guo, F., Cerullo, I., Chen, X., & Rosbash, M. (2014). PDF neuron firing phase-shifts key circadian activity neurons in *Drosophila*. *Elife*, *3*, e02780.

Hadjieconomou, D., Rotkopf, S., Alexandre, C., Bell, D. M., Dickson, B. J., & Salecker, I. (2011). Flybow: Genetic multicolor cell labeling for neural circuit analysis in *Drosophila melanogaster*. *Nature Methods*, *8*, 260–266.

Hamblen-Coyle, M. J., Wheeler, D. A., Rutila, J. E., Rosbash, M., & Hall, J. C. (1992). Behavior of period-altered Circadian Rhythm Mutants of *Drosophila* in Light: Dark Cycles (Diptera: *Drosophilidae*). *Journal of Insect Behavior*, *5*, 417–446.

Handler, A. M., & Konopka, R. J. (1979). Transplantation of a circadian pacemaker in *Drosophila*. *Nature*, *279*, 236–238.

Harper, R. E., Dayan, P., Albert, J. T., & Stanewsky, R. (2016). Sensory conflict disrupts activity of the *Drosophila* circadian network. *Cell Reports*, *17*, 1711–1718.

Helfrich, C., & Engelmann, W. (1983). Circadian rhythm of the locomotor activity in *Drosophila melanogaster* and its Mutants 'Sine Oculis' and 'Small Optic Lobes'. *Physiological Entomology*, *8*, 257–272.

Helfrich-Förster, C., & Homberg, U. (1993). Pigment-dispersing hormone-immunoreactive neurons in the nervous system of wild-type *Drosophila melanogaster* and of several mutants with altered circadian rhythmicity. *Journal of Comparative Neurology*, *8*, 177–190.

Helfrich-Förster, C. (1995). The period clock gene is expressed in central nervous system neurons which also produce a neuropeptide that reveals the projections of circadian pacemaker cells within the brain of *Drosophila melanogaster*. *Proceedings of the National Academy of Sciences of United States of America*, *92*, 612–616.

Helfrich-Förster, C. (1998). Robust circadian rhythmicity of *Drosophila melanogaster* requires the presence of lateral neurons: A brain-behavioral study of disconnected mutants. *The Journal of Comparative Physiology*, *182*, 435–453.

Helfrich-Förster, C., Edwards, T., Yasuyama, K., Wisotzki, B., Schneuwly, S., Stanewsky, R., … Hofbauer, A. (2002). The extraretinal eyelet of *Drosophila*: Development, ultrastructure, and putative circadian function. *Journal of Neuroscience*, *22*, 9255–9266.

Helfrich-Förster, C. (2003). The neuroarchitecture of the circadian clock in the brain of *Drosophila melanogaster*. *Microscopy Research and Technique*, *62*, 94–102.

Helfrich-Förster, C., Shafer, O. T., Wülbeck, C., Grieshaber, E., Rieger, D., & Taghert, P. (2007). Development and morphology of the clock-gene-expressing lateral neurons of *Drosophila melanogaster*. *The Journal of Comparative Neurology*, *500*, 47–70.

Hendricks, J. C., Finn, S. M., Panckeri, K. A., Chavkin, J., Williams, J. A., Sehgal, A., & Pack, A. I. (2000). Rest in *Drosophila* is a sleep-like state. *Neuron*, *25*, 129–138.

Hendricks, J. C., Lu, S., Kume, K., Yin, J. C. P., Yang, Z., & Sehgal, A. (2003). Gender dimorphism in the role of cycle (BMAL1) in rest, rest regulation, and longevity in *Drosophila melanogaster*. *Journal of Biological Rhythms*, *18*, 12–25.

Hermann-Luibl, C., Yoshii, T., Senthilan, P. R., Dircksen, H., & Helfrich-Förster, C. (2014). The ion transport peptide is a new functional clock neuropeptide in the fruit fly *Drosophila melanogaster*. *Journal of Neuroscience*, *34*, 9522–9536.

Hofbauer, A. (1991). *Eine Bibliothek monoklonaler Antikörper gegen das Gehirn von Drosophila melanogaster*. Würzburg: University of Würzburg.

Homberg, U., Davis, N. T., & Hildebrand, J. G. (1991a). Peptide-immunocytochemistry of neurosecretory cells in the brain and retrocerebral complex of the spinx moth *Manduca sexta*. *The Journal of Comparative Neurology*, *303*, 35–52.

Homberg, U., Wurden, S., Dircksen, H., & Rao, K. R. (1991b). Comparative anatomy of pigment dispersing hormone-immunoreactive neurons in the brain of orthopteroid insects. *Cell Tissue Research*, *266*, 343–357.

Homberg, U., Reischig, T., & Stengl, M. (2003). Neural organization of the circadian system of the cockroach *Leucophaea maderae*. *Chronobiology International*, *20*, 577–591.

Im, S. H., Li, W., & Taghert, P. H. (2011). PDFR and CRY signaling converge in a subset of clock neurons to modulate the amplitude and phase of circadian behavior in *Drosophila*. *PLoS One*, *6*, e18974.

Jefferis, G. S., Potter, C. J., Chan, A. M., Marin, E. C., Rohlfing, T., Maurer, C. R., & Luo, L. (2007). Comprehensive maps of *Drosophila* higher olfactory centers: Spatially segregated fruit and pheromone representation. *Cell*, *128*, 1187–1203.

Jenett, A., Rubin, G. M., Ngo, T. T., Sheperd, D., Murphy, C., Dionne, H., … Zugates, C.T. (2012). A *Gal4*-driver line resource for *Drosophila* neurobiology. *Cell Reports*, *2*, 991–1001.

Johard, H. A., Yoshii, T., Dircksen, H., Cusumano, P., Rouyer, F., Helfrich-Förster, C., & Nässel, D. R. (2009). Peptidergic clock neurons in *Drosophila*: Ion transport peptide and short neuropeptide F in subsets of dorsal and ventral lateral neurons. *The Journal of Comparative Neurology*, *516*, 59–73.

Kaneko, M., Helfrich-Förster, C., & Hall, J. C. (1997). Spatial and temporal expression of the period and timeless genes in the developing nervous system of *Drosophila*: Newly identified pacemaker candidates and novel features of clock gene product cycling. *Journal of Neuroscience*, *17*, 6745–6760.

Kaneko, M., & Hall, J. C. (2000). Neuroanatomy of cells expressing clock genes in *Drosophila*: Transgenic manipulation of the period and timeless genes to mark the perikarya of circadian pacemaker neurons and their projections. *The Journal of Comparative Neurology*, *422*, 66–94.

Kaneko, H., Head, L. M., Ling, J., Tang, X., Liu, Y., Hardin, P. E., … Hamada, F. N. (2012). Circadian rhythm of temperature preference and its neural control in *Drosophila*. *Current Biology*, *22*, 1851–1857.

King, A. N., Barber, A. F., Smith, A. E., Dreyer, A. P., Sitaraman, D., Nitabach, M. N., … Sehgal, A. (2017). A peptidergic circuit links the circadian clock to locomotor activity. *Current Biology*, *27*, 1915–1927.

Konopka, R. J., & Benzer, S. (1971). Clock mutants of *Drosophila melanogaster*. *Proceedings of the National Academy of Sciences of the United States of America*, *68*, 2112–2116.

Liang, X., Holy, T. E., & Taghert, P. H. (2016). Synchronous *Drosophila* circadian pacemakers display nonsynchronous Ca^{2+} rhythms *in vivo*. *Science*, *351*, 976–981.

Liang, X., Holy, T. E., & Taghert, P. H. (2017). A series of suppressive signals within the *Drosophila* circadian neural circuit generates sequential daily outputs. *Neuron*, *94*, 1173–1189.

Liu, T., Mahesh, G., Houl, J. H., & Hardin, P. E. (2015). Circadian activators are expressed days before they initiate clock function in late pacemaker neurons from *Drosophila*. *Journal of Neuroscience*, *35*, 8662–8671.

Lyons, L. C., & Roman, G. (2009). Circadian modulation of short-term memory in *Drosophila*. *Learning & Memory*, *16*, 19–27.

Manoli, D. S., Foss, M., Villella, A., Taylor, B. J., Hall, J. C., & Baker, B. S. (2005). Male-specific fruitless specifies the neural substrates of *Drosophila* Courtship behaviour. *Nature*, *436*, 395–400.

Myers, E. M., Yu, J., & Sehgal, A. (2003). Circadian control of eclosion Interaction between a central and peripheral clock in *Drosophila melanogaster*. *Current Biology*, *13*, 526–533.

Nicolaï, L. J., Ramaekers, A., Raemaekers, T., Drozdzecki, A., Mauss, A. S., Yan, J., … Hassan, B. A. (2010). Genetically encoded dendritic marker sheds light on neuronal connectivity in *Drosophila*. *Proceedings of the National Academy of Sciences of United States of America*, *107*, 20553–20558.

Omoto, J. J., Keleş, M. F., Nguyen, B. C. M., Bolanos, C., Lovick, J. K., Frye, M. A., & Hartenstein, V. (2017). Visual input to the *Drosophila* central complex by developmentally and functionally distinct neuronal populations. *Current Biology*, *27*, 1098–1110.

Parisky, K. M., Agosto, J., Pulver, S. R., Shang, Y., Kuklin, E., Hodge, J. J., … Griffith, L. C. (2008). PDF Cells are a GABA-responsive wake-promoting component of the *Drosophila* sleep circuit. *Neuron*, *60*, 672–682.

Park, D., & Griffith, L. C. (2006). Electrophysiological and anatomical characterization of PDF-positive clock neurons in the intact adult *Drosophila* brain. *Journal of Neurophysiology*, *95*, 3955–3960.

Peng, H., Ruan, Z., Long, F., Simpson, J. H., & Myers, E. W. (2010). V3D enables real-time 3D visualization and quantitative analysis of large-scale biological image data sets. *Nature Biotechnology*, *28*, 348–353.

Peng, H., Bria, A., Zhou, Z., Iannello, G., & Long, F. (2014a). Extensible visualization and analysis for multidimensional images using Vaa3D. *Nature Protocols*, *9*, 193–208.

Peng, H., Tang, J., Xiao, H., Bria, A., Zhou, J., Butler, V., … Long, F. (2014b). Virtual finger boosts three-dimensional imaging and microsurgery as well as terabyte volume image visualization and analysis. *Nature Communications*, *5*, 4342.

Petsakou, A., Sapsis, T. P., & Blau, J. (2015). Circadian rhythms in rho1 activity regulate neuronal plasticity and network hierarchy. *Cell*, *162*, 823–835.

Pfeiffer, B. D., Jenett, A., Hammonds, A. S., Ngo, T. T., Misra, S., Murphy, C., … Rubin, G. M. (2008). Tools for neuroanatomy and neurogenetics in *Drosophila*. *Proceedings of the National Academy of Sciences of the United States of America*, *105*, 9715–9720.

Pfeiffer, B. D., Ngo, T. T., Hibbard, K. L., Murphy, C., Jenett, A., Truman, J. W., & Rubin, G. M. (2010). Refinement of tools for targeted gene expression in *Drosophila*. *Genetics*, *186*, 735–755.

Picot, M., Klarsfeld, A., Chélot, E., Malpel, S., & Rouyer, F. (2009). A role for blind DN2 clock neurons in temperature entrainment of the *Drosophila* larval brain. *Journal of Neuroscience*, *29*, 8312–8320.

Pittendrigh, C. S., & Skopik, S. D. (1970). Circadian systems, V. The driving oscillation and the temporal sequence of development. *Proceedings of the National Academy of Sciences of Unites Staes of America*, *65*, 500–507.

Pittendrigh, C. S., & Daan, S. (1976). A functional analysis of circadian pacemakers in nocturnal rodents. *Journal of Comparative Neurology*, *106*, 291–331.

Pírez, N., Christmann, B. L., & Griffith, L. C. (2013). Daily rhythms in locomotor circuits in *Drosophila* involve PDF. *Journal of Neurophysiology*, *110*, 700–708.

Potdar, S., & Sheeba, V. (2012). Large ventral lateral neurons determine the phase of evening activity peak across photoperiods in *Drosophila melanogaster*. *Journal of Biological Rhythms*, *27*, 267–279.

Reischig, T., & Stengl, M. (2003). Ectopic transplantation of the accessory medulla restores circadian locomotor rhythms in arrhythmic cockroaches (*Leucophaea maderae*). *Journal of Experimental Biology*, *206*, 1877–1886.

Renn, S. C., Park, J. H., Rosbash, M., Hall, J. C., & Taghert, P. H. (1999). A *pdf* neuropeptide gene mutation and ablation of PDF neurons each cause severe abnormalities of behavioral circadian rhythms in *Drosophila*. *Cell*, *99*, 791–802.

Rideout, E. J., Dornan, A. J., Neville, M. C., Eadie, S., & Goodwin, S. F. (2010). Control of sexual differentiation and behavior by the doublesex gene in *Drosophila melanogaster*. *Nature Neuroscience*, *13*, 458–466.

Rieger, D., Shafer, O. T., Tomioka, K., & Helfrich-Förster, C. (2006). Functional analysis of circadian pacemaker neurons in *Drosophila melanogaster*. *Journal of Neuroscience*, *26*, 2531–2543.

Robinett, C. C., Vaughan, A. G., Knapp, J. M., & Baker, B. S. (2010). Sex and the single-cell. II. There is a time and place for sex. *PLoS Biology*, *8*, e1000365.

Rohlfing, T., & Maurer, C. R. (2003). Nonrigid image registration in shared-memory multiprocessor environments with application to brains, breasts, and bees. *IEEE Transactions on Information Technology in Biomedicine*, *7*, 16–25.

Rowell, H. F. (1976). The cells of the insect neurosecretory system: Constancy, variability, and the concept of the unique identifiable neuron. *Advances in Insect Physiology*, *12*, 63–123.

Rulifson, E. J., Kim, S. K., & Nusse, R. (2002). Ablation of insulin-producing neurons in flies: Growth and diabetic phenotypes. *Science*, *296*, 1118–1120.

Sakai, T., & Ishida, N. (2001). Circadian rhythms of female mating activity governed by clock genes in *Drosophila*. *Proceedings of the National Academy of Sciences United States of America* , *98*, 9221–9225.

Schindelin, J., Arganda-Carreras, I., Frise, E., Kaynig, V., Longair, M., Pietzsch, S., … Cardona, A. (2012). Fiji: An open-source platform for biological-image analysis. *Nature Methods*, *9*, 676–682.

Schlichting, M., Menegazzi, P., Lelito, K. R., Yao, Z., Buhl, E., Dalla Benetta, E., … Shafer, O. T. (2016). A neural network underlying circadian entrainment and photoperiodic adjustment of sleep and activity in *Drosophila*. *Journal of Neuroscience*, *36*, 9084–9096.

Schmid, B., Schindelin, J., Cardona, A., Longair, M., & Heisenberg, M. (2010). A high-level 3D visualization API for Java and ImageJ. *BMC Bioinformatics*, *11*, 274.

Sehadova, H., Glaser, F. T., Gentile, C., Simoni, A., Giesecke, A., Albert, J. T., & Stanewsky, R. (2009). Temperature entrainment of *Drosophila's* circadian clock involves the gene nocte and signaling from peripheral sensory tissues to the brain. *Neuron*, *64*, 251–266.

Sehgal, A., Price, J. L., Man, B., & Young, M. W. (1994). Loss of circadian behavioral rhythms and per RNA oscillations in the *Drosophila* mutant timeless. *Science*, *263*, 1603–1605.

Selcho, M., Mill'an, C., Palacios-Munoz, A., Ruf, F., Ubillo, L., Chen, J., … Ewer, J. (2017). Central and peripheral clocks are coupled by a neuropeptide pathway in *Drosophila*. *Nature Communications*, *8*, 15563.

Shafer, O. T., Helfrich-Förster, C., Renn, S. C. P., & Taghert, P. H. (2006). Reevaluation of *Drosophila melanogaster's* neuronal circadian pacemakers reveals new neuronal classes. *The Journal of Comparative Neurology*, *498*, 180–193.

Shang, Y., Donelson, N. C., Vecsey, C. G., Fang, G., Rosbash, M., & Griffith, L. C. (2013). Short neuropeptide F is a sleep-promoting inhibitory modulator. *Neuron*, *80*, 171–183.

Shaw, P. J., Cirelli, C., Greenspan, R. J., & Tononi, G. (2000). Correlates of sleep and waking in *Drosophila melanogaster*. *Science (New York, N. Y.)*, *287*, 1834–1837.

Sheeba, V., Gu, H., Sharma, V. K., O'Dowd, D. K., & Holmes, T. C. (2008). Circadian-and light-dependent regulation of resting membrane potential and spontaneous action potential firing of *Drosophila* circadian pacemaker neurons. *Journal of Neurophysiology*, *99*, 976–988.

Shimosako, N., Hadjieconomou, D., & Salecker, I. (2014). Flybow to dissect circuit assembly in the *Drosophila* brain. *Methods in Molecular Biology (Clifton, N.J.)*, *1082*, 57–69.

Sidote, D., Majercak, J., Parikh, V., & Edery, I. (1998). Differential effects of light and heat on the *Drosophila* circadian clock proteins PER and TIM. *Molecular and Cellular Biology*, *18*, 2004–2013.

Siegmund, T., & Korge, G. (2001). Innervation of the ring gland of *Drosophila melanogaster*. *The Journal of Comparative Neurology*, *431*, 481–491.

Sivachenko, A., Li, Y., Abruzzi, K. C., & Rosbash, M. (2013). The transcription factor Mef2 links the *Drosophila* core clock to Fas2, neuronal morphology, and circadian behavior. *Neuron*, *79*, 281–292.

Stoleru, D., Peng, Y., Agosto, J., & Rosbash, M. (2004). Coupled oscillators control morning and evening locomotor behaviour of *Drosophila*. *Nature*, *431*, 862–868.

Tang, X., Roessingh, S., Hayley, S. E., Chu, M. L., Tanaka, N. K., Wolfgang, W., … Hamada, F. N. (2017). The role of PDF neurons in setting the preferred temperature before dawn in *Drosophila*. *eLife*, *6*, e23206.

Tauber, E., Roe, H., Costa, R., Hennessy, J. M., & Kyriacou, C. P. (2003). Temporal mating isolation driven by a behavioral gene in *Drosophila*. *Current Biology*, *13*, 140–145.

Veelaert, D., Schoofs, L., & De Loof, A. (1998). Peptidergic control of the corpus cardiacum-corpora allata complex of locusts. *International Review of Cytology*, *182*, 249–302.

Veleri, S., Rieger, D., Helfrich-Förster, C., & Stanewsky, R. (2007). Hofbauer-Buchner eyelet affects circadian photosensitivity and coordinates TIM and PER expression in *Drosophila* clock neurons. *Journal of Biological Rhythms*, *22*, 29–42.

Xiao, H., & Peng, H. (2013). APP2: Automatic tracing of 3D neuron morphology based on hierarchical pruning of a gray-weighted image distance-tree. *Bioinformatics*, *29*, 1448–1454.

Xu, K., Zheng, X., & Sehgal, A. (2008). Regulation of feeding and metabolism by neuronal and peripheral clocks in *Drosophila*. *Cell Metabolism*, *8*, 289–300.

Xu, K., DiAngelo, J. R., Hughes, M. E., Hogenesch, J. B., & Sehgal, A. (2011). The circadian clock interacts with metabolic physiology to influence reproductive fitness. *Cell Metabolism*, *13*, 639–654.

Yao, Z., & Shafer, O. T. (2014). The *Drosophila* circadian clock is a variably coupled network of multiple peptidergic units. *Science*, *343*, 1516–1520.

Yoshii, T., Sakamoto, M., & Tomioka, K. (2002). A temperature-dependent timing mechanism is involved in the circadian system that drives locomotor rhythms in the fruit fly *Drosophila melanogaster*. *Zoological Science*, *19*, 841–850.

Yoshii, T., Heshiki, Y., Ibuki-Ishibashi, T., Matsumoto, A., Tanimura, T., & Tomioka, K. (2005). Temperature cycles drive *Drosophila* circadian oscillation in constant light that otherwise induces behavioural arrhythmicity. *European Journal of Neuroscience*, *22*, 1176–1184.

Yoshii, T., Todo, T., Wülbeck, C., Stanewsky, R., & Helfrich-Förster, C. (2008). Cryptochrome is present in the compound eyes and a subset of *Drosophila*'s clock neurons. *The Journal of Comparative Neurology*, *508*, 952–966.

Yoshii, T., Vanin, S., Costa, R., & Helfrich-Förster, C. (2009). Synergic entrainment of *Drosophila's* circadian clock by light and temperature. *Journal of Biological Rhythms*, *24*, 452–464.

Yu, J. Y., Kanai, M. I., Demir, E., Jefferis, G. S. X. E., & Dickson, B. J. (2010). Cellular organization of the neural circuit that drives *Drosophila* courtship behavior. *Current Biology*, *20*, 1602–1614.

Zaretsky, M., & Loher, W. (1983). Anatomy and electrophysiology of individual neurosecretory cells of an insect brain. *The Journal of Comparative Neurology*, *216*, 253–263.

Zhang, Y. Q., Rodesch, C. K., & Broadie, K. (2002). Living synaptic vesicle marker: Synaptotagmin-GFP. *Genesis (New York, N.Y. : 2000)*, *34*, 142–145.

Zhou, C., Franconville, R., Vaughan, A. G., Robinett, C. C., Jayaraman, V., & Baker, B. S. (2015). Central neural circuitry mediating courtship song perception in male *Drosophila*. *eLife*, *4*, e08477.

How to cite this article: Schubert FK, Hagedorn N, Yoshii T, Helfrich-Förster C, Rieger D. Neuroanatomical details of the lateral neurons of *Drosophila melanogaster* support their functional role in the circadian system. *J Comp Neurol*. 2018;526:1209–1231. https://doi.org/10.1002/cne.24406